

ScholarWorks@GSU

Enhanced Electrochemiluminescence and Current Signals from Metal Nanoclusters and Their Surface Assemblies by Prototype Tertiary Amines

| | |
|---------------|--|
| Authors | Yi, Meijun |
| Citation | Yi, Meijun. "Enhanced Electrochemiluminescence and Current Signals from Metal Nanoclusters and Their Surface Assemblies by Prototype Tertiary Amines." Thesis, Georgia State University, 2019. https://doi.org/10.57709/15940334 |
| DOI | https://doi.org/10.57709/15940334 |
| Download date | 2026-04-10 23:29:55 |
| Link to Item | https://hdl.handle.net/20.500.14694/2945 |

ENHANCED ELECTROCHEMILUMINESCENCE AND CURRENT SIGNALS FROM
METAL NANOCLUSTERS AND THEIR SURFACE ASSEMBLIES BY PROTOTYPE
TERTIARY AMINES

by

MEIJUN YI

Under the Direction of Gangli Wang, PhD

ABSTRACT

Interactions between metal nanoclusters and tertiary amine compounds are demonstrated to generate and strengthen the near infrared electrochemiluminescence (ECL) and current signals upon electrode activation. The catalytic effects of aqueous soluble gold nanoclusters (Au NCs) on the oxidation of prototype tertiary amine are firstly established in solution measurements with the materials system of Au₂₂ lipoic acid (Au-LA) nanoclusters and a common pH buffer HEPES. The near IR ECL and current signals are correlated by potential scanning and step methods under systematic varied HEPES and nanocluster concentrations. Strategies to deposit the nanoclusters on electrode surface are developed to improve the signal and enhancement for future applications. The deposition strategies are further applied to prepare surface assemblies of

organic soluble bimetallic $\text{Au}_{25-x}\text{Ag}_x$ nanoclusters with controlled morphology and coverage. Piperazine derivative drug cetirizine is found to enhance ECL signals from this bimetallic nanocluster-functionalized electrode devices that can be further developed for sensing applications.

INDEX WORDS: Electrochemistry, ITO electrode, Near-Infrared luminescence, Au nanoclusters, Fluorescence microscopy imaging

ENHANCED ELECTROCHEMILUMINESCENCE AND CURRENT SIGNALS FROM
METAL NANOCLUSTERS AND THEIR SURFACE ASSEMBLIES BY PROTOTYPE
TERTIARY AMINES

by

MEIJUN YI

A Thesis Submitted in Partial Fulfillment of the Requirements for the Degree of

Master of Science

in the College of Arts and Sciences

Georgia State University

2019

Copyright by
Meijun Yi
2019

ENHANCED ELECTROCHEMILUMINESCENCE AND CURRENT SIGNALS FROM
METAL NANOCLUSTERS AND THEIR SURFACE ASSEMBLIES BY PROTOTYPE
TERTIARY AMINES

by

Meijun Yi

Committee Chair: Gangli Wang

Committee: Kathryn Grant

Shahab A Shamsi

Electronic Version Approved:

Office of Graduate Studies

College of Arts and Sciences

Georgia State University

December 2019

DEDICATION

The thesis is dedicated to my beloved grandfather, Chengfang Yi, who passed away this year. My mother, Ping Wang, who inspired me with her positive attitude and unconditional love. My family and all my friends that encouraged and supported me along the way. My advisor Dr. Gangli Wang for the opportunity to join his lab and guidance.

ACKNOWLEDGMENTS

I want to thank Dr. Gangli Wang for all the guidance, patience, and encouragement that was given. Former lab members Dr. Tanyu Wang and Dr. Jonathan W. Padelford for the training of making microelectrode sensors and academic advices in the field of chemistry. Current member Maksim M. Kvetny, Hedi Ma, and Michael Messinger for the training and care over time and help that lead to creation to this thesis. Also, my committed members Dr. Shahab A Shamsi and Dr. Kathryn Grant for their time and feedback. Last, but not least, I'd like to thank Dr. Ning Fang and his lab for giving me the opportunity to work with their spin coater instrument.

TABLE OF CONTENTS

| | | |
|---|--|-------------|
| ACKNOWLEDGMENTS | | V |
| LIST OF FIGURES | | X |
| LIST OF ABBREVIATIONS | | XVII |
| 1 INTRODUCTION | | 1 |
| 1.1 Electrochemical Biosensors | | 1 |
| <i>1.1.1 Basic principles and applications of electrochemical sensors</i> | | <i>1</i> |
| <i>1.1.2 Surface material and modifications</i> | | <i>3</i> |
| <i>1.1.3 Surface modification methods via solution deposition</i> | | <i>4</i> |
| 1.2 Electrochemical Detection Techniques | | 6 |
| <i>1.2.1 Amperometric and voltammetric techniques</i> | | <i>6</i> |
| <i>1.2.2 Near IR electrogenerated chemiluminescence</i> | | <i>6</i> |
| 1.3 Basic Introduction of Noble Metal Nanoclusters | | 7 |
| <i>1.3.1 Molecular-like gold nanocluster</i> | | <i>8</i> |
| <i>1.3.2 Bimetallic nanoclusters</i> | | <i>9</i> |
| 2 ELECTROCHEMILUMINESCENCE AND CURRENT AS DUAL SIGNALS IN THE ELECTROCHEMICAL DETECTION BASED ON AU NANOCCLUSERS.. | | 9 |
| 2.1 Abstract | | 9 |
| 2.2 Background and Strategy | | 10 |
| 2.3 Experimental Details | | 12 |

| | | |
|-------|---|----|
| 2.3.1 | <i>Materials</i> | 12 |
| 2.3.2 | <i>Synthesis of aqueous Au nanoclusters stabilized by lipoic acid (LA)</i> | 12 |
| 2.3.3 | <i>Near IR Electrogenenerated chemiluminescence measurements</i> | 13 |
| 2.3.4 | <i>Electrochemical measurements</i> | 14 |
| 2.3.5 | <i>Microscopy imaging</i> | 14 |
| 2.3.6 | <i>Surface treatment of ITO electrode</i> | 15 |
| 2.4 | Results and Discussion | 16 |
| 2.4.1 | <i>Electrochemical oxidation of HEPES with ITO electrodes catalyzed by Au-LA nanoclusters in aqueous solution</i> | 16 |
| 2.4.2 | <i>Calibration profiles of HEPES as prototype in the presence of Au-LA nanocluster in aqueous solution at physiological pH</i> | 18 |
| 2.4.3 | <i>Current and ECL responses by varying AuNCs concentration in fixed HEPES concentration</i> | 25 |
| 2.4.4 | <i>Surface deposition of AuNCs film on ITO electrodes as integrated detection platform</i> | 29 |
| 2.5 | Conclusion | 36 |
| 3 | SURFACE ASSEMBLY OF Au₁₂Ag₁₃ BIMETALLIC NANOCCLUSERS ON ITO ELECTRODES: NEAR IR ELECTROCHEMILUMINESCENCE AND OPTICAL IMAGING | 38 |
| 3.1 | Abstract | 38 |
| 3.2 | Background and Strategy | 38 |

| | | |
|------------|--|-----------|
| 3.3 | Experimental Details..... | 41 |
| | 3.3.1 <i>Materials.....</i> | 41 |
| | 3.3.2 <i>ITO electrode preparation</i> | 42 |
| | 3.3.3 <i>Electrochemical measurements.....</i> | 42 |
| | 3.3.4 <i>Near IR Electrogenerated chemiluminescence measurements.....</i> | 42 |
| | 3.3.5 <i>Microscopy imaging.....</i> | 43 |
| | 3.3.6 <i>Dip coating method.....</i> | 43 |
| | 3.3.7 <i>Spin coating method.....</i> | 43 |
| 3.4 | Results and Discussion..... | 44 |
| | 3.4.1 <i>Au₁₂Ag₁₃ nanocluster modified ITO electrode surface.....</i> | 44 |
| | 3.4.2 <i>The enhancement of surface near IR ECL signal by tertiary amine containing drug cetirizine</i> | 48 |
| | 3.4.3 <i>Surface distribution and morphologies of Au₁₂Ag₁₃ NCs on ITO electrodes by spin coating with mixed solvents</i> | 51 |
| 3.5 | Conclusion..... | 56 |
| 4 | SUMMARY | 57 |
| | REFERENCES | 59 |

LIST OF FIGURES

| | |
|--|-----------|
| <i>Figure 1.1 Dip coating steps of (1) dipping, (2) substrate immersion/dwell into the precursor solution and (3) pulling at a constant speed.</i> | <i>4</i> |
| <i>Figure 1.2 Spin coating process with dynamic dispense.</i> | <i>5</i> |
| <i>Figure 2.1. Molecular structure of Au₂₂-LA₁₂ and HEPES.</i> | <i>13</i> |
| <i>Figure 2.2 The 3-electrode system in quartz cuvette for ECL measurement. The cuvette cap is placed on the top responsible for maintaining the proximal position of the three electrodes.</i> | <i>14</i> |
| <i>Figure 2.3 . Cyclic voltammograms of ITO electrode in 100 mM HEPES at pH 7.4 (black), 50 μM Au-LA (red), 50 μM Au-LA and 100 mM HEPES at pH 7.4 (blue).</i> | <i>16</i> |
| <i>Figure 2.4 Cyclic voltammograms of ITO electrode in 1 mM ferrocene with 0.1 M TBAP as supporting electrolyte from -0.2 V to 1.2 V at scan rate 0.1 V/s</i> | <i>17</i> |
| <i>Figure 2.5 The dependence of current signal on HEPES concentration measured by (A) Cyclic voltammetry and (B) Square wave voltammetry. The test solution contains 50 μM Au-LA at pH 7.4 with 0.2 M NaClO₄ as electrolyte. The scan rate in CV was 0.1 V/s. In SWV, frequency 25 Hz, pulse size 25 mV and step size 2 mV were used.</i> | <i>18</i> |
| <i>Figure 2.6 Overlay of the peak current from CV and SWV at different HEPES concentrations. The peak current values were read at around 0.75 V. Blue squares are SWV data and red spheres are from CV. Error bar is the standard deviation of three repeating measurement cycles. Zoom-in with HEPES concentration in log scale shows the lower concentration trend.</i> | <i>19</i> |
| <i>Figure 2.7 Near IR ECL signal at different HEPES concentrations. Data were measured under ambient condition without degas. of the measurement solution contains 50 μM Au-LA at</i> | |

- pH 7.4 with 0.2 M NaClO₄ as electrolyte. The electrode potential was held for 2s at -0.8 V and then step to 1.2 V for 6 s for 10 repeated cycles. Zoom-in of the first cycle is plotted to better illustrate the peak shape and steady-state plateau toward the end of the cycle.* 20
- Figure 2.8 The near IR ECL signal dependence on HEPES concentration. The solution contains 50 μM Au-LA with 0.2 M NaClO₄ as supporting electrolyte. ECL intensity at 8 s was averaged over ten cycles at each concentration (data from Fig. 2.6). Error bar is the standard deviation of ten repeating measurement cycles. Dash line is a linear fitting in approximation.* 22
- Figure 2.9 Current vs time profile for near IR ECL. The electrode potential was held for 2s at -0.8 V and then step to 1.2 V for 6 s for 10 cycles. The bottom panel zooms in the first cycle to illustrate the plateau current.* 23
- Figure 2.10 Correlation of the steady state ECL intensity and current at different HEPES concentrations. Error bar is the standard deviation. The current (red sphere) and ECL (blue square) signals are taken at the same time point, i.e. at 5th second then every 8 s (13th s, 21st s, 29th s, 37th s... data from Fig. 2.7 & Fig. 2.9).* 24
- Figure 2.11 The dependence of anodic current on Au-LA concentration in (A) CV and (B) SWV. Data collected in 100 mM HEPES at pH 7.4 with 0.2 M NaClO₄. The CV scan rate was 0.1 V/s. The frequency 25 Hz, pulse size 25 mV and step size 2 mV were used in SWV... 26*
- Figure 2.12 The dependence of current from CV and SWV on Au-LA NCs concentration. Current values were read at the peak around 0.75 V for each concentration in Fig. 2.11. Red spheres and blue squares are CV and SWV respectively.*..... 26
- Figure 2.13 Near IR ECL signal at different AuLA NCs concentrations. The electrode potential was held for 2s at -0.8 V and then step to 1.2 V for 6 s over 10 repeated cycles.* 27

- Figure 2.14 Analysis of ECL intensity (results in Fig. 2.13). The steady-state intensity at the plateau is averaged over ten cycles as reference. The left panel compare to the 1st peak, while the right panel compares to the average peak intensity of the following nine cycles. Linear fitting of all three data sets has an $R^2 > 0.9$ 28*
- Figure 2.15 CV-ECL profiles of bare ITO (left) and ITO with Au-LA NCs film (right). Black curve is current from CV (left axis) and red is ECL intensity (right axis). Tested in 25 mM HEPES with 0.2 M NaClO₄ solution at pH 7.4. The current and ECL scales are set the same in the two panels for direct comparison. 29*
- Figure 2.16 UV-Vis spectra of ZnCl₂ titration in 25 mM HEPES (left), 50 μM Au-LA in 25 mM HEPES (right) with 0.2 M NaClO₄..... 31*
- Figure 2.17 ECL characterization of AuNCs film deposited over different incubation period of (A) 30 mins (B) 2 hours with first cycle zoom-in (C) 12 hours. The ITO electrodes were soaked in 1 mM ZnCl₂ with 50 μM Au-LA and 25 mM HEPES for AuNC film preparation. The ECL was measured in different HEPES solutions containing 0.2 M NaClO₄ as supporting electrolytes and 1 mM ZnCl₂ to suppress film dissolution. The electrode potential was held for 2s at -0.8 V and then step to +1.2 V for 6 s for 4 cycles. Measured under ambient condition without degas..... 32*
- Figure 2.18 Analysis of ECL performance of different AuNCs films in representative HEPES concentrations from data in Fig. 2.17. The integrated ECL signal (left) was calculated from the sum area of the ECL intensity in one cycle. The ECL signal at steady state (right) was from data at 3s after +1.2V was applied. The symbol and error bar are the mean and standard deviation from the four repeated cycles in each measurement. 33*

Figure 2.19 fluorescence microscopic imaging and stability of AuNCs film on ITO electrodes:

(A) after 2-hour incubation/deposition; (B) after ECL measurements in 25 mM HEPES with 1 mM ZnCl₂ (C) after ECL measurements in 25 mM HEPES without ZnCl₂. The brightness and contrast of the images were set consistently for direct comparison. (D) The step ECL profiles of film stability in 1 mM ZnCl₂ with 25 mM HEPES. The electrode potential was held for 2s at -0.8 V and then step to 1.2 V for 6 s for 4 cycles. Measured under ambient condition without degas. 34

Figure 2.20 ECL signals from AuNCs film drop cast on ITO electrode tested in 0.2 M NaClO₄ electrolyte only (red, bottom curve) and 25 mM HEPES with 0.2 M NaClO₄ electrolyte (black, top curve). A 10 μL precipitating solution containing 50 μM Au-LA and 2mM ZnCl₂ with 25 mM HEPES was dropcast on ITO and air dried. The electrode potential was held for 2s at -0.8 V and then step to 1.2 V for 6 s for 50 cycles. Measured under ambient condition without degas. 35

Figure 3.1 X-ray structure of rod-shape Ag₁₃Au₁₂ nanoclusters (NCs)⁴⁴ 39

Figure 3.2 Spectroscopic features of Au₁₂Ag₁₃ in solution: ECL and PL spectra (left) and UV-vis absorption spectrum (right). The ECL spectrum was collected with 10 μM Au₁₂Ag₁₃ and 1 mM TPrA under +1.0 V. The PL nanocluster sample is about 10 times less concentrated without TPrA. The PL spectrum profile was corrected. (Take from ref. ⁴³) 40

Figure 3.3 Cetirizine dihydrochloride structure..... 41

Figure 3.4 . The step ECL signals from different surface deposition methods. The stock NCs DCM solution was used in all three preparations. Tested in PBS buffer at pH 7.4. The electrode potential was held for 0.3s at -1.0 V and then stepped to 1.0 V for 0.1s. No

- potential was applied after 2.3s. Inset better illustrates the low intensity signals (first cycle excluded)..... 45
- Figure 3.5 fluorescence microscopic imaging of surface deposited NCs by spin coating (left) 10 drops and (right) 25 drops of 5 μ L stock DCM solution. Spin coating speed was 600 RPM. Near IR photoluminescence from the NCs using 377 \pm 50 nm excitation filter and 647 nm long pass emission filter pass filter and a 40X objective. The contrast/brightness is set the same for all images. 46
- Figure 3.6 Fluorescence imaging of (left) Bare ITO surface (middle) Dip coating with instant dipping (right) Dip coating with 5 minutes incubation. Bright features are the near IR photoluminescence from the NCs. Images recorded using 377 \pm 50 nm excitation filter and 647 nm long pass emission filter and a 40X objective. The contrast/brightness is set the same for all images. 47
- Figure 3.7 The CV-ECL curves of AgAu NCs deposited on ITO working electrode tested without (left) and with (right) 1 mM cetirizine in PBS buffer pH 7.4 . Cyclic voltammogram current in black on left axis, ECL intensity in blue on right axis. 48
- Figure 3.8 Step ECL signals with and without 1 mM Cetirizine in pH 7.4 PBS buffer. The electrode potential was held for 0.3s at -1.0 V (starting from zero second) and then stepped to 1.0 V for 0.1s cyclically. Data with four repeated cycles are plotted. The NCs were deposited by adding 5 μ L drop of stock DCM solution under spin coating speed of 600 RPM ten times. 49
- Figure 3.9 Consistency in step ECL signals with respect to the surface deposition: (left) 1st peak and (right) the 3rd peak intensity with cetirizine drug (black) and without (red). The x-axis represents different concentrations of Au₁₂Ag₁₃ NCs used in the spin coating process,

- with 100% corresponding to the stock solution. Each point represents a separate film/measurement like those in Fig. 3.7 (original data not shown). 50
- Figure 3.10 Fluorescence (left) and bright field (right) images of surface assembled NCs prepared by spin coating with 1:1 of ACN:DCM as mixed solvent at spin speed 600 RPM. Three drops of 3 μ L solution was used to form the microcrystal assembly..... 51
- Figure 3.11 ECL profile of the NCs microcrystals (shown in Fig. 3.9) in 1 mM Cetirizine (black) and without cetirizine (red) in pH 7.4 PBS buffer. Insert is zoom-in of later four cycles for better demonstration the ECL signal without cetirizine. The electrode potential was held for 0.3s at -1.0 V and then step to 1.0 V for 0.1s cyclically. 52
- Figure 3.12 , Fluorescence images of surface assembled NCs prepared by spin coating with 1:1 DCM: chloroform as mixed solvent at spin speed 600 RPM (left) and 900 RPM (right). 53
- Figure 3.13 ECL profile of the surface assembled NCs prepared by spin coating with 1:1 DCM: chloroform as mixed solvent. Measured in 1 mM Cetirizine in pH 7.4 PBS buffer. The electrode potential was held for 0.3s at -1.0 V and then step to 1.0 V for 0.1s cyclically.53
- Figure 3.14 The homogeneity analysis of NCs film on ITO. The top left panel provides an overview of ITO slide including the physical edge under fluorescence (left) and bright field (right) mode. The two fluorescence images at the bottom provide zoom-in area of (A) the edge of the NCs film; and (B) the interior of the NCs film. Spin coating speed was 900 RPM. Scale bar size is 100 μ m in all images. The two-line profiles in analysis (C) are the emission intensity along the yellow arrows in image A and B respectively. Distance zero is the start of the arrow from the left. NCs film prepared by spin coating a single 3 μ L drop NCs solution with 1: 1 DCM: chloroform solvent. 55

LIST OF ABBREVIATIONS

| | |
|--------------------|--|
| Au DTCs | Gold DiThiolate Clusters |
| Au MPCs | Gold Monolayer-Protected Clusters |
| Au MTCs | Gold Mixed Thiolate Clusters |
| Au NCs | Gold nanoclusters |
| Au NPs | Gold nanoparticles |
| ACN | Acetonitrile |
| CV | Cyclic Voltammetry |
| DPV | Differential Pulse Voltammetry |
| DCM | Methylene Chloride or Dichloromethane |
| EDL | Electrical Double Layer |
| FT-IR | Fourier-Transform Infrared Spectroscopy |
| HOMO | Highest Occupied Molecular Orbital |
| LA | Lipoic Acid |
| LUMO | Lowest Unoccupied Molecular Orbital |
| MS | Mass Spectrometry |
| NaClO ₄ | Sodium Perchlorate |
| NCs | Nanoclusters |
| NPs | Nanoparticles |
| PBS | Phosphate Buffered Solution |
| QE | Quantum Efficiency |
| RCA-1 | Radio Corporation of America Standard Cleaning Procedure 1 |
| SP AuNPs | Surface Plasmonic Gold Nanoparticles |

| | |
|--------|----------------------------------|
| SWV | Square Wave Voltammetry |
| TBAP | Tetrabutylammonium Perchlorate |
| TEM | Transmission Electron Microscopy |
| TOABr | Tetraoctylammonium Bromide |
| UV | Ultraviolet |
| UV-Vis | Ultraviolet-Visible |
| Vis | Visible |

1 INTRODUCTION

1.1 Electrochemical Biosensors

Biosensors are integrated devices that transform bio-information into physicochemical signals as output for detection¹. The samples in biosensor detection can be non-physiological sample or biospecimen such as blood, urine and other body fluidics or samples. Various biosensors have been or are being developed which all have common components: the biochemical receptor or recognition system; the transducer system; and signal processing and analysis system². The specificity of biosensors is often based on the receptor recognition to a specific target compound as analyte. Antibodies, nucleic acids, enzymes and their biomimetics are common receptors that are assembled on transducer surfaces. The transducers generate optical, mass-based, electrochemical or other types of physical signals upon the recognition of the target^{3, 4}. The signals are either processed and analyzed as direct output, such as glucose level from a glucometer, or through interface with computer/cell phone/instruments. Electrochemical biosensors are uniquely advantageous over other signal generation mechanism because the hardware is relatively inexpensive, and the biological information is directly converted into electronic signals at the electrode surface²⁻⁶. The electrochemical detection techniques are discussed further in section 1.2.

1.1.1 Basic principles and applications of electrochemical sensors

Like most electrochemical measurements, electrochemical sensing normally requires a three-electrode system: a working (sensing) electrode, a reference electrode and a counter electrode⁷. The working electrode is where the reaction of interest takes place. The most common conductive material for working electrodes include metals such as gold, platinum, carbon in various forms, metal oxides etc. An instrument called potentiostat is used to control

and measure the potential or current in the chemical/biological system. For analysis purpose in electroanalytical measurements, the working electrode should be inert within the applied potential range in which the solvent should remain nonreactive or noninterfering. A reference electrode is needed to provide a constant potential value against which the potential on the working electrode is adjusted or measured⁷. Although the standard potentials of redox species are reported in reference to standard hydrogen electrode (SHE), saturated calomel electrode (SCE) and Ag/AgCl electrode are commonly used instead of SHE as reference electrodes for simplicity (by avoiding hydrogen gas). The current flows through working and counter electrodes and is often quantitatively correlated with the analyte amount or concentration as calibration type responses¹.

The most known and successful electrochemical biosensors would be glucose test strips or alike⁸. Several generations of sensor design for glucose testing have been developed over the past decades, all requiring the amplification of electrochemical current signals by redox enzyme/s (glucose oxidase). Other redox enzymes with suitable substrates or conjugated through antibodies are also frequently used in the development of various chemical or biological sensors⁹.¹⁰. An essential step is the selection of working electrode materials and correspondingly electrode surface functionalization methods. It is worth emphasizing that current is a rate term, i.e. concentration/amount per time. Therefore, electrochemical measurements are intrinsically kinetics limited/involved, or dependent of the heterogeneous electron transfer and mass transport at the electrode-solution interface⁶. The performance of an electrochemical sensor will highly depend on the quality of the electrode surface functions.

1.1.2 Surface material and modifications

The choices of electrode material and surface modification strategy highly depend on the nature of the interested target molecule/s and the application needs. Chemical modification such as self-assembly monolayer (SAM) of thiols on gold is probably one of the most used electrode functionalization strategies due to the strong Au-S bonding or monolayer stability¹¹⁻¹³.

Physisorption is also widely used for simplicity and readiness, especially in many electrode-materials systems where covalent bonding is not feasible or unfavorable.

Indium tin oxide (ITO) electrodes are chosen in this thesis research because of the high optical transparency and electrochemical conductivity. ITO has been widely used in combined electrochemical and spectroscopic measurements. It is a wideband gap semiconductor electrode prepared by coating a mixture of In_2O_3 and SnO_2 on an inert glass support¹⁴. The as prepared ITO surface is relatively hydrophobic on which non-polar film or organic soluble materials readily adsorb or deposit. To increase the wettability of the surface in aqueous environment, different surface treatments such as etching have been developed to make more hydrophilic surface by introducing functional groups/sites such as hydroxyls¹⁵⁻¹⁸. Surface treatments, especially aggressive etch for cleaning and activation, will have strong impact on the ITO sensor efficiency but should not change the electronic properties of ITO surface¹⁴. For hydroxylated ITO surface, samples in aqueous solution can be applied and filmed onto ITO surface via self-assembly -monolayer (SAM) process. Representative examples are enzymes or protein antibodies as biological recognition elements. Attaching organic molecular on bare/inactivated ITO surface is also reported as strongly and rapidly physi-sorbed. The efficiency of the surface-functionalized ITO sensors highly depend on the quality of the film, including the deposited amount/surface concentration and uniformness, on the ITO surface. Meanwhile, the quality of

the thin film on ITO strongly depends on the surface treatment and the deposition method that generally require optimization.

1.1.3 Surface modification methods via solution deposition

Spin coating and dip coating methods are among the most common and easily accessible wet chemical deposition methods. Both approaches are adopted in this thesis. The basic principle and procedure are described next.

Dip coating process is sketched in Figure 1.1. The simple procedure is more suitable for qualitative exploratory tests. Still, the immerse time, pulling speed and solvent evaporation rate and the sample concentration should all be considered for the reproducibility of the surface film formation¹⁹. A longer immersion/dwell time could allow better interaction or adsorption of the precursor solution on the substrate. A thin layer solution could form during the pulling process, during which evaporation could cause further deposition of precursor species. The speed of pulling is related to the solvent evaporating rate will affect the uniformness and coverage of the precursor film. Excess solution is generally drained/airdried form the surface after it was pulled out.

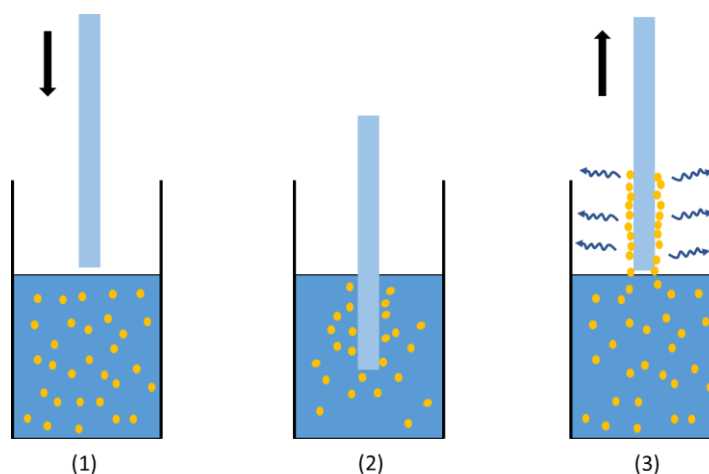


Figure 1.1 Dip coating steps of (1) dipping, (2) substrate immersion/dwell into the precursor solution and (3) pulling at a constant speed.

Spin coating method is one of the most common techniques to deposit uniform thin films. It has widespread applications in film manufacturing. The process is quick, reproducible and relatively easy to operate once the condition is established²⁰. The general procedure is shown in Figure 1.2. The coating material is dissolved in a solvent and dropped on a rotating substance (ITO electrode) surface during step 1. Extra material solution is sheared on the surface and flung off under a high-speed rotation (≥ 600 rpm) shown in step 2. The solvent is dried by the airflow during spinning while the solute materials deposit on the surface (step 3). At last the film forms after the solvent fully dries out and leave coating material on the surface (step 4). Spin coating methods requires very low material volume and short preparation time. However, non-uniform amorphous film could form at fast drying for solvent with high evaporating rate²⁰. Solvents with slow evaporation rates and low rotation speed could be beneficial to fabricate uniform films by increasing the time for the coating materials to self-assemble on the surface.

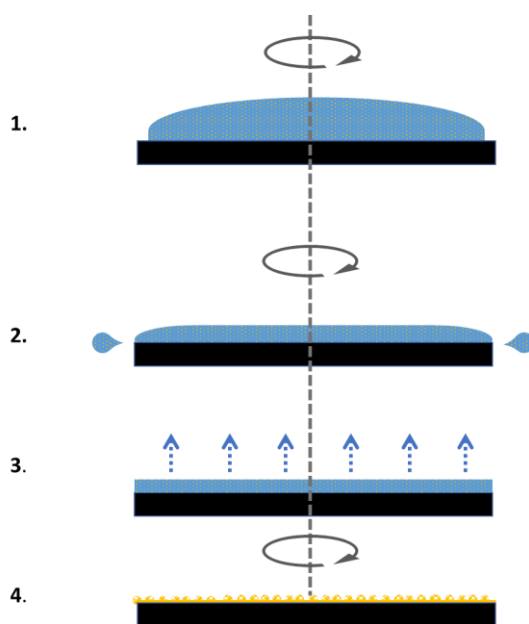


Figure 1.2 Spin coating process with dynamic dispense.

1.2 Electrochemical Detection Techniques

The basic electrochemical methods directly relevant to this thesis is briefly described next.

1.2.1 *Amperometric and voltammetric techniques*

The amperometry technique measures current over time under constant applied potential/s. A redox reaction usually is happening on the working electrode surface. Most amperometric sensors detect steady-state current as signal that is normally proportional to the concentration of the electroactive species². Voltammetric techniques such as potential-scanning cyclic voltammetry (CV) and potential-stepped/pulsed square wave voltammetry (SWV) are used to investigate the mechanism, electron transfer kinetics and detection of low signals etc^{2, 6, 21}. In SWV, the charging current, background interference signal in most amperometric and voltammetric measurements, is greatly eliminated through the data sampling and analysis enabled by the pulse potential waveform. The high sensitivity of SWV makes it favorable in sensing measurements for improved signal-to-noise ratio or detection limit.

1.2.2 *Near IR electrogenerated chemiluminescence*

Electrochemiluminescence or electrogenerated chemiluminescence, abbreviated as ECL, refers to the photoemission activated by electrode reactions²². ECL is a sub-category of chemiluminescence and has been studied since the 1960s^{22, 23}. ECL can be activated by either oxidation or reduction of the redox active ECL reagents at controlled electrode potentials. There are two major pathways for ECL generation: self-annihilation ECL and coreactant ECL. In either pathway, ECL is generated when the excited species (R^*) return to the ground state via photoemission or radiative decay. The excited species (R^*) is formed through the annihilation of the oxidized and reduced ECL reagent (R). In self-annihilation ELC, both oxidized and reduce

intermediates, often radical cation (R^+) and radical anion (R^-), are generated through consecutive heterogeneous oxidation and reduction reactions driven by electrode. With coreactants, one electrode reaction, either oxidation or reduction, will oxidize or reduce both the ECL reagent and the coreactants. The oxidized (or reduced) coreactants then undergo follow-up reactions to become reductant (or oxidant) which will react with the oxidized (or reduced) ECL reagent and form the excited species (R^*). The corresponding coreactant ECL is named as oxidative-reduction ECL or reductive-oxidation ECL respectively^{22, 24}.

As a relatively low cost and simple platform, ECL is employed in many analytical applications as signal generation/readout in immunoassays and sensing²⁵. ECL in near IR region is gaining attention recently for the benefit of less background interference particularly in biomedical settings. Near IR ECL reagents with high efficiency remain to be developed. Some gold and other metal nanoclusters (AuNCs) have high quantum efficiency of near IR photoluminescence. Near IR ECL from several organic soluble AuNCs through coreactant pathway has been reported by Ding's group²⁶. By using good's buffer 4-(2-Hydroxyethyl)-1-Piperazineethanesulfonic Acid (HEPES) and chelator EDTA as coreactants at physiological pH, near IR ECL from aqueous soluble AuNCs has been reported by our group^{27, 28}. A new mechanism to enhance the ECL efficiency is also introduced by covalently attaching multiple coreactants onto the ligands of a nanocluster such that charge transfers after electrode activation become intra-cluster rather than via diffusional collisions²⁸.

1.3 Basic Introduction of Noble Metal Nanoclusters

Over the past decades, nanomaterials have been extensively investigated as an explosive research area by engineers, physicists, chemists, material scientists. Nanomaterials generally refer

to those with at least one-dimension less than one hundred nanometers. Various materials including semiconductors, noble metal and carbon etc. have been explored²⁹⁻³¹. An important feature is the quantum confinement effect that makes these nanomaterials uniquely different from atoms or macroscopic materials^{30, 32, 33}. Accordingly, the optical, electrochemical and other properties of nanomaterials are size, shape and interface dependent.

1.3.1 Molecular-like gold nanocluster

Gold is known to be inert as noble metal. In 1857, Faraday was the first to report the synthesis of gold colloid by reducing gold chloride aqueous solution by phosphorus in CS₂, and he was able to detect gold particles by light scattering³². The low toxicity concern makes gold materials highly advantageous in biomedical applications. For centuries, the drinkable gold particles have been used for the curative purposes and also as glass colorant agents³². While there is no definitive cutoff sizes, gold colloids, gold nanoparticles or other nanosized shapes, and nanoclusters follow the trend of decreasing sizes.

Nanoclusters are generally composed of a metal core less than 2-3 nanometer in diameter that is stabilized by organic compounds referred as ligands¹³. A stricter definition would be the opening of an energy gap in electronic structure. In 1994, a seminal two-phase synthesis method was reported by Brust-Schiffrin to prepare gold clusters with thiols^{13, 32, 34}. The strong gold-sulfur bonding ensures a monolayer of thiolate ligands to stabilize the gold cores from further aggregation and decomposition. Discrete numbers of Au atoms in the core and ligands in the monolayer, often referred as magic numbers in earlier literature, define different so-called monolayer-protected clusters (MPCs)³².

1.3.2 Bimetallic nanoclusters

The metal core in nanoclusters can be monometallic such as Au, Ag, or bimetallic or alloys². A large variety of alloy and hybrid materials have been explored to produce different properties. There are two major ways to prepare a bimetallic core: co-reduction of mixed ions and successive reduction of two metal salts^{35,36}. In the co-reduction process, two corresponding metal ions are being simultaneously reduced and stabilized chemically. This method provides less predictable coordination of the bimetallic cluster structure. In the successive reduction method, the deposition or exchange of one metal on the other pre-formed metal precursor forms a core-shell or alloy like bimetallic core³⁶.

2 ELECTROCHEMILUMINESCENCE AND CURRENT AS DUAL SIGNALS IN THE ELECTROCHEMICAL DETECTION BASED ON AU NANOCCLUSERS

2.1 Abstract

Electrochemical properties of aqueous soluble gold nanoclusters are employed to establish dual-signal detection strategies. Oxidation of a prototype tertiary amine, the common pH buffer HEPES, with ITO electrode is found catalyzed by lipoic acid stabilized Au₂₂ nanoclusters (NCs). The process corresponds to the widely adopted coreactant oxidative-reduction ECL pathways and enhances the ECL signal from the Au NCs. The near IR ECL from the AuNCs and the redox current are demonstrated to depend on the solution concentrations of both species. The surface deposition of AuNCs on ITO electrodes is performed to simplify the signal generation processes and enhance the signals. The AuNC-modified ITO electrode surface is also characterized by microscopy imaging taking advantage of the photoluminescence of the

AuNCs. Results in this chapter provide principles and strategies to develop sensor type devices for future applications such as the detection of tertiary amine containing drugs or biomarkers.

2.2 Background and Strategy

Many piperazine drugs contain tertiary amine structures that can function as efficient coreactants to enhance the ECL signals. The HEPES as a prototype the representative tertiary amine buffer is detected with ITO electrode in aqueous solution at physiological pH. The surface modified ITO electrode for HEPES detection is able to produce sufficient near IR ECL with a low money and timely cost. The stability of modified ITO electrode surface is demonstrated by photoluminescence microscopy imaging. The solution catalytic effects enabled and motivated the surface-immobilized NCs on ITO electrode for ECL-Current measurement as dual signals.

Multi-modal signals offer advantages to reduce possible false positive/negative results which are critical in the analysis of samples with high interference such as biofluids. Among various electrochemical methods, electrochemiluminescence (ECL) in near infrared (IR) is far less exploited. Near IR spectrum window is appealing due to less background interference and simple instrumentation. Our group among others have reported strong photoluminescence and ECL from thiolate stabilized Au nanoclusters^{26, 37}. Method development and applications based on both ECL and current signals remain to be demonstrated.

ECL is activated by electrode reactions of ECL reagent/s not by light source. Another reagent, often referred as coreactant, can be added to react with the ECL reagent after the electrode activation of both ECL reagent and coreactant. The coreactant pathway, compared to the self-annihilation (i.e. without coreactant), offers much stronger ECL signals for detection but requires high excess coreactant/s. $\text{Ru}(\text{bpy})_3^{2+}$ (bpy = 2,2'-bipyridine) and tri-n-propylamine

(TPrA) is the most used oxidative-reduction ECL system in sensor development and commercial assays²². The visible ECL from Ru(bpy)₃ is enhanced by the oxidized tertiary amine in TPrA under appropriate conditions. The requirement of antibody for recognition and redox enzymes for signal amplification significantly limit the scope of applications.

Aqueous soluble Au NCs have received significant research attention for their photoluminescence in near IR and biocompatibility. Recently, the self-annihilation near IR ECL of Au₂₂-LA₁₂ nanocluster, and the coreactant ECL pathway of Au₂₂-LA₁₂ with tertiary amine containing coreactants have been reported by our group²⁶⁻²⁸. The tertiary amine containing coreactant, common chelator EDTA and pH buffer HEPES, enhances the near IR ECL from AuNCs. Since many metal ion chelators and drugs contain tertiary amine structures, both redox current and ECL can be generated as signal-on detection strategies by optimizing the measurement parameters such as electrode potential ranges. The types of electrode materials, its function), AuNCs, and prototype tertiary amine as analyte/coreactant are chosen to: 1. correlate the redox current with near IR ECL as dual signals; 2. design and optimize the measurement parameters; 3. establish the detection strategy/principle for future applications.

The indium tin oxide (ITO) coated thin glass is chosen as the electrode in this project for the combined optical transparency and electrical conductivity. ITO is widely used in solar cells and electronics due to its high transparency at the visible range and high conductance^{17, 38}. Its surface deposition method has been widely studied for sensing purposes. Generally speaking, functional materials are deposited on ITO substrate to construct sensor type devices. Because the sensor efficiency and consistency can be highly dependent on the uniformity of the deposited film on the ITO surface, the surface treatment of ITO and the deposition method need to be optimized based on the property of the to-be-deposited materials to ensure film quality.

Diffusional reactions of AuNCs and HEPES in solution measurements are firstly studied with ITO electrode. The AuNCs are then deposited on ITO surface under different methods and conditions. The assembled ITO-AuNCs device is used to measure HEPES as a prototype analyte to demonstrate the signal-on responses.

2.3 Experimental Details

2.3.1 Materials

Tetrachloroauric acid trihydrate ($\text{HAuCl}_4 \cdot 3\text{H}_2\text{O}$, >99.99%), lipoic acid (LA, $\geq 99\%$), sodium borohydride (NaBH_4 , $\geq 99\%$), sodium hydroxide (NaOH , $\geq 97\%$), 4-(2-Hydroxyethyl) piperazine-1-ethanesulfonic acid or N-(2-Hydroxyethyl) piperazine-N-(2-ethanesulfonic acid) (HEPES, $\geq 99.5\%$), sodium perchlorate hydrate ($\text{NaClO}_4 \cdot x\text{H}_2\text{O}$, $\geq 99.99\%$), Zinc Chloride (ZnCl_2 , $\geq 98\%$), sodium phosphate monobasic (NaH_2PO_4 , $\geq 99.5\%$) and sodium phosphate dibasic (Na_2HPO_4 , $\geq 99\%$) were purchased from Sigma-Aldrich and used as received. Ferrocene, ($\text{FeC}_{10}\text{H}_{10}$, $\geq 99\%$) was purchased from Alfa Aesar and used as received. (In all solution preparations, nanopure water (>18 M Ω cm) from a Barnstead system was used.

2.3.2 Synthesis of aqueous Au nanoclusters stabilized by lipoic acid (LA)

The synthesis follows previously reported procedure with modifications^{28, 37, 39, 40}. Hydrogen tetrachloroaurate ($\text{HAuCl}_4 \cdot 3\text{H}_2\text{O}$) was prepared with the concentration of 0.006 M; and the lipoic acid solution was prepared with concentration of 0.035 M in nanopour water. The pH of lipoic acid was adjusted to basic with 0.5 M NaOH to fully dissolve lipoic acid prior of mixing. Two solutions were vigorously stirred for 4 hours upon mixing to the Au:LA final ratio of 1:3. By the end the solution mixture turned from light yellow to colorless. Then NaBH_4 was

added in the mixture and stirred for about 17 hours until the near IR photoluminescence emission reaches the maximum. The final Au-LA nanocluster solution was dialysis over 4 days then the solvent was removed by rotovap at 40 °C.

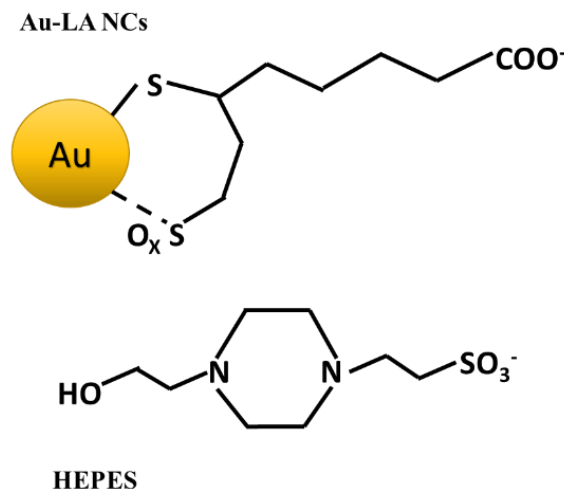


Figure 2.1. Molecular structure of Au₂₂-LA₁₂ and HEPES.

2.3.3 Near IR Electrogenerated chemiluminescence measurements

The ECL was measured in a quartz cuvette (Scheme1). A 3-D printed spectrometer cuvette holder was used to hold the cuvette in front of the camera window at a fixed position. An ITO electrode (Delta Technologies) was positioned in the light path at a fix position by wiring the working electrode connection through a cap fitting on the top of the cuvette to ensure consistent electrode-camera alignment. The supporting electrolyte was 0.2 M NaClO₄. For results to be directly relevant to real life broader application settings, all measurements were performed under ambient conditions without degassing. Unless defined otherwise, the electrode potential was held for 2s at -0.8 V and then stepped to 1.2 V for 6 s. The emission intensity was recorded with an Andor iDUS CCD camera (Model DU401A-BR-DD). To synchronize the camera and electrical potential, the camera is externally triggered by the potentiostat (Gamry

Reference 600) at time zero when the potential is applied. The ECL intensity is the sum of photon counts from all pixels; the exposure time is 15 ms for step ECL measurement unless otherwise noted.

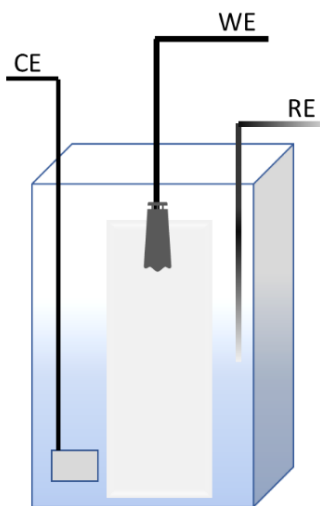


Figure 2.2 The 3-electrode system in quartz cuvette for ECL measurement. The cuvette cap is placed on the top responsible for maintaining the proximal position of the three electrodes.

2.3.4 Electrochemical measurements

Cyclic voltammograms were collected using a potentiostat (Gamry Reference 600) in Faraday Cage with Ag/AgCl as a quasi-reference electrode, platinum (Pt) foil as a counter electrode and ITO as a working electrode. Scan rate was set with 0.1 V/s for all current measurements. The supporting electrolyte was 0.2 M NaClO₄.

2.3.5 Microscopy imaging

A fluorescence microscope (Olympus IX73) was used for ITO film imaging. An 377+/- 50 nm band pass filter for excitation and 647 nm long pass filter for emission were used to record

the fluorescence images with 33 ms exposure time. The excitation light source is a high-power LED light (Excelitas Technology, X-Cite 120 LED Boost)

2.3.6 Surface treatment of ITO electrode

The ITO slides were first cleaned with a general cleaning process by ultrasonically in nanopure water, ethanol and nanopure water (1:3), and nanopure water for at least 15 minutes each. The RCA-1 (Radio Corporation of America Standard Cleaning Procedure 1) process was used to change the surface hydrophobicity for better wettability in aqueous solution and affinity to polar species^{14, 17, 18}. Briefly, an ITO electrode was soaked in a 5:1:1 solution of H₂O: H₂O₂: NH₄OH for 1 hour at 70°C, then rinsed thoroughly with water, and again immersed into ethanol and nanopure water (1:3) and ultrasonically for at least 15 minutes. After the surface treatment, the ITO electrode is used in the study referred as bare ITO.

2.4 Results and Discussion

2.4.1 Electrochemical oxidation of HEPES with ITO electrodes catalyzed by Au-LA nanoclusters in aqueous solution

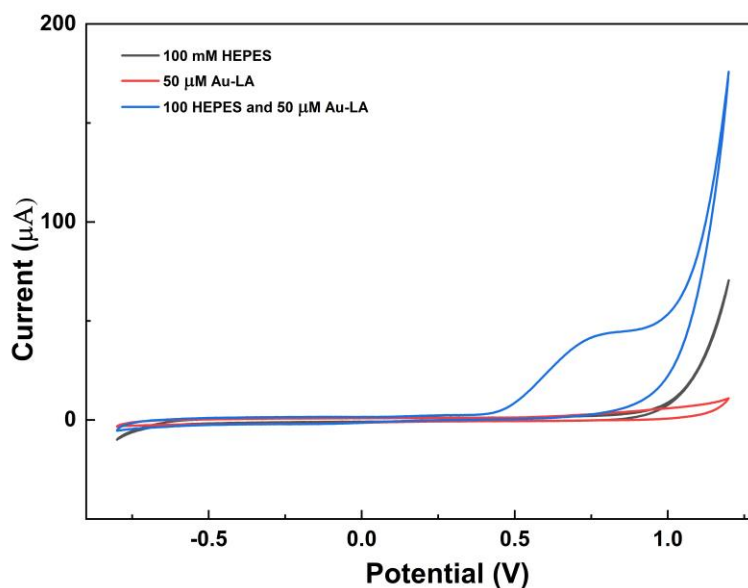


Figure 2.3 . Cyclic voltammograms of ITO electrode in 100 mM HEPES at pH 7.4 (black), 50 μM Au-LA (red), 50 μM Au-LA and 100 mM HEPES at pH 7.4 (blue).

The catalytic effect of Au₂₂-LA₁₂ nanocluster for the oxidation of HEPES on ITO electrode is established first for the development of detection methodology based on nanoclusters such as Au₂₂-LA₁₂. HEPES as a common physiological buffer can be oxidized at around 0.75 V versus Ag/AgCl on glassy carbon electrode²⁸. However, on ITO electrode, only when both Au₂₂-LA₁₂ and HEPES are present, a totally irreversible oxidation peak at around 0.75 V is observed shown in Fig. 2.3. As controls, neither 50 μM Au₂₂-LA₁₂ with electrolyte nor 100 mM HEPES alone display comparable redox current. This is likely due to the sluggish electron transfer kinetics which requires a large overpotential to drive the electron transfer reactions on ITO electrodes. The results demonstrate that HEPES oxidation is mediated or catalyzed by the Au₂₂-LA₁₂ which is the first catalytic activity to the best of our knowledge. The mechanism, in

principle, allows the development of signal-on type electrochemical detections in which the current signal is quantitatively correlated with the target. Further, since the oxidation of tertiary amine in HEPES is expected to enhance the near IR ECL of the AuNCs through the coreactant ECL pathways, both redox current and ECL will be the signals enhanced by appropriated tertiary amines at a respective potential ranges.

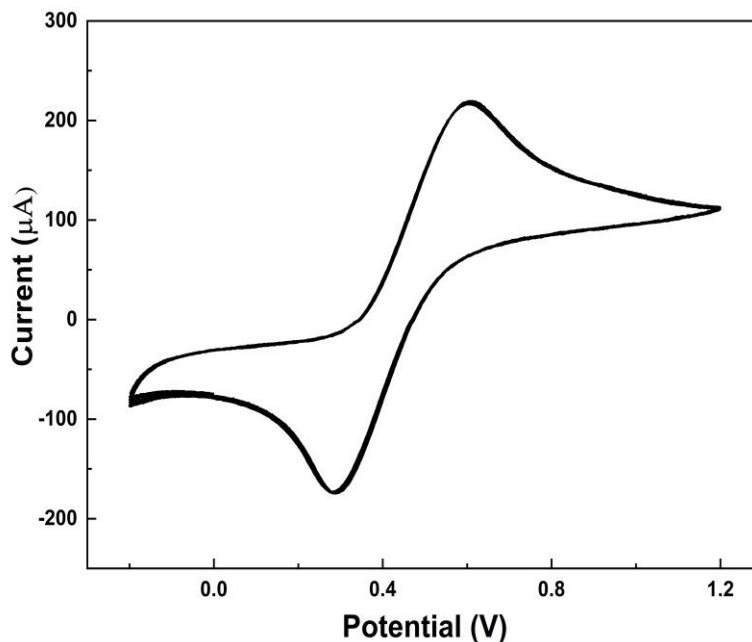
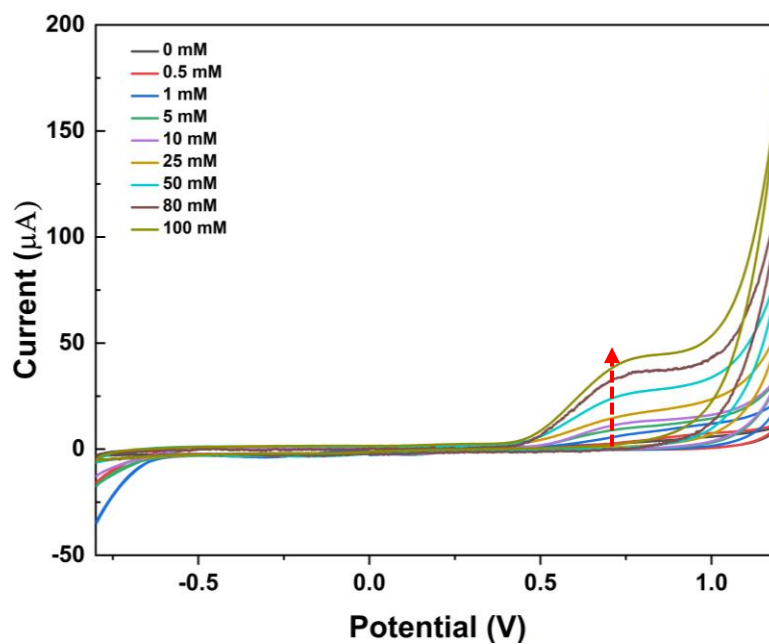


Figure 2.4 Cyclic voltammograms of ITO electrode in 1 mM ferrocene with 0.1 M TBAP as supporting electrolyte from -0.2 V to 1.2 V at scan rate 0.1 V/s

To calibrate both the electrode potential and the effective area of ITO, the bare ITO electrode was tested in 1 mM ferrocene acetonitrile solution. Fig 2.4 shows an oxidation peak at around 0.6 V and the reversal reduction peak around 0.3 V. The quasi to totally irreversible redox peaks from ferrocene, one of the fastest electron transfer kinetics known, confirms the sluggish electron transfer rate on ITO. The peak current value I_p is ca. 2.2×10^4 A. Using the the Randles-Sevcik equation⁷, the calculated area of ITO electrode is around 0.6 cm².

2.4.2 Calibration profiles of HEPES as prototype in the presence of Au-LA nanocluster in aqueous solution at physiological pH

(A)



(B)

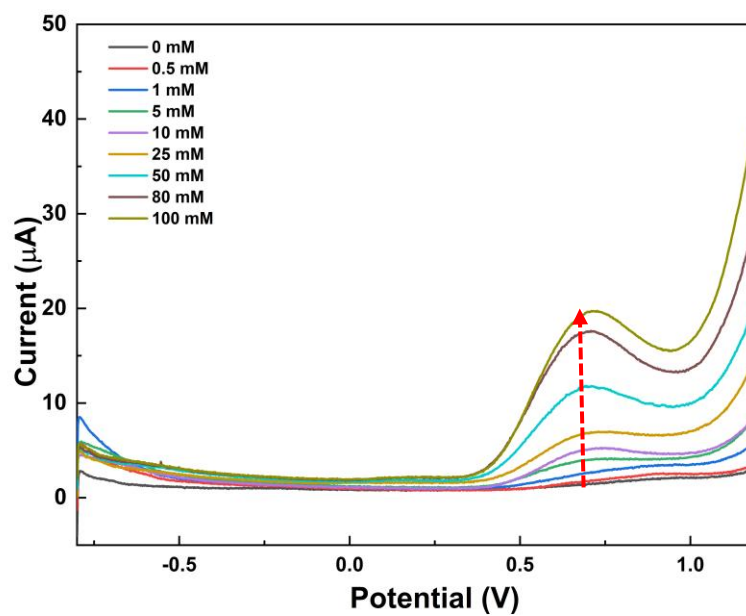


Figure 2.5 The dependence of current signal on HEPES concentration measured by (A) Cyclic voltammetry and (B) Square wave voltammetry. The test solution contains $50 \mu\text{M}$ Au-LA

at pH 7.4 with 0.2 M NaClO₄ as electrolyte. The scan rate in CV was 0.1 V/s. In SWV, frequency 25 Hz, pulse size 25 mV and step size 2 mV were used.

With no coreactant, i.e. zero HEPES concentration in the solution, there is a very weak oxidation current of Au-LA nanocluster at around 0.9 V in both the CV and SWV. At increasing HEPES concentrations, the oxidation peak at around 0.75 V increases accordingly. The oxidation and reduction branches in a CV curve provide mechanistic insights. No reduction features were observed in all CV curves over a large potential range, which suggest the oxidation process is chemically irreversible. Pulse voltammetry such as SWV provides the benefit of better background suppression and higher sensitivity. From the oxidation scans in SWV, the lower detection limit of 0.5 mM HEPES is achieved. The detection will be limited by the noise level and can be significantly improved upon further method optimization for a real analyte/sample.

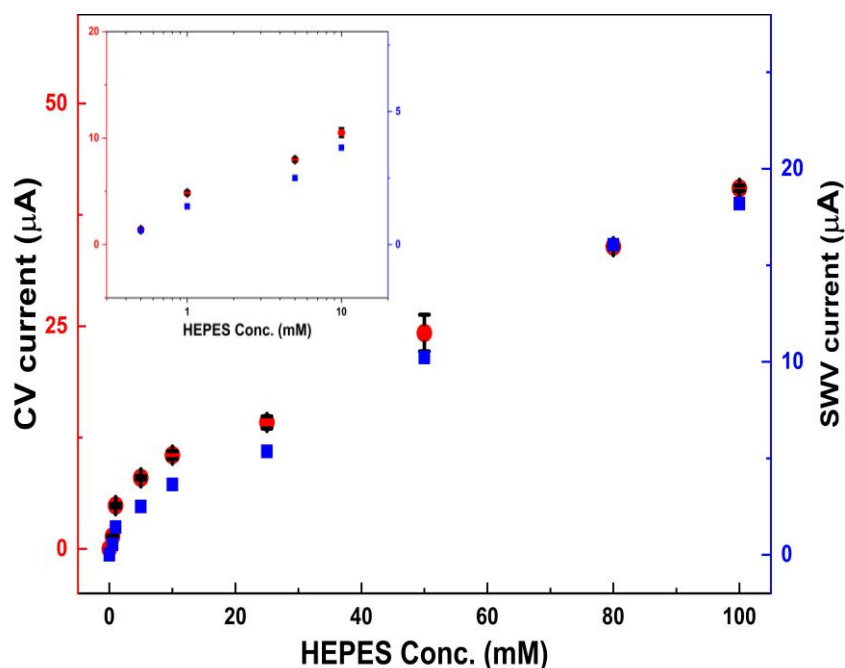


Figure 2.6 Overlay of the peak current from CV and SWV at different HEPES concentrations. The peak current values were read at around 0.75 V. Blue squares are SWV data and red spheres are from CV. Error bar is the standard deviation of three repeating measurement cycles. Zoom-in with HEPES concentration in log scale shows the lower concentration trend.

The peak currents from CV and SWV are plotted in Fig. 2.5 as proof of principle calibration profiles. The peak current increases with the HEPES concentration at a steeper rate at the lower range, then more gradual and linear at higher concentration range. At the lower concentration range with the log scale for x-axis, a more linear relationship between the concentration and signal intensity is established. The trend is likely resulted from the diffusional reactions of the two species (AuNCs at 50 μM and HEPES at higher concentrations) which require further studies. Regardless, the same trend from two different methods (CV and SWV) strongly suggest the current as promising sensing signals catalyzed by the trace amount of AuNCs.

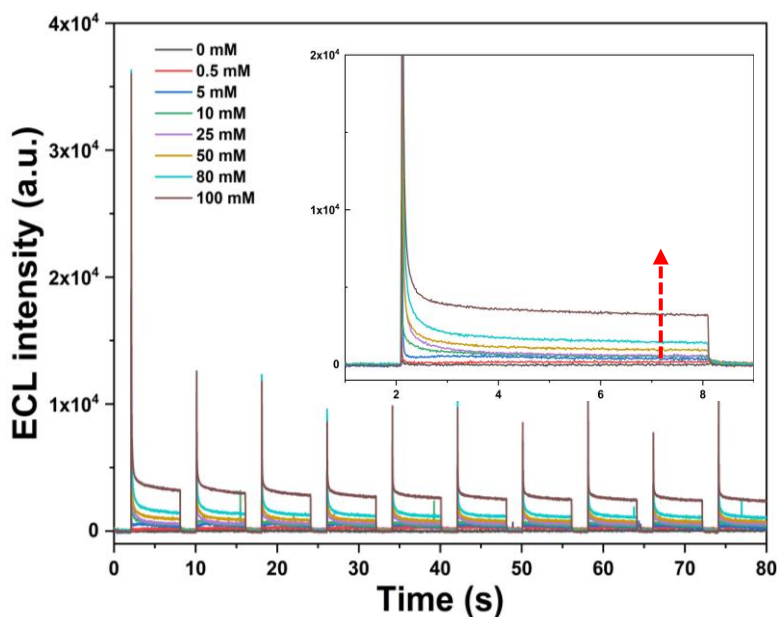


Figure 2.7 Near IR ECL signal at different HEPES concentrations. Data were measured under ambient condition without degas. of the measurement solution contains 50 μM Au-LA at pH 7.4 with 0.2 M NaClO_4 as electrolyte. The electrode potential was held for 2s at -0.8 V and then step to 1.2 V for 6 s for 10 repeated cycles. Zoom-in of the first cycle is plotted to better illustrate the peak shape and steady-state plateau toward the end of the cycle.

Next, calibration based on ECL signal is performed under comparable solution conditions. In this experiment, HEPES as a good's buffer with moderate oxidation potential was

used also as the coreactant to enhance the ECL signals. Because quaternary ammonium ions are known ineffective to enhance the ECL as coreactants, the pKa of amine groups and solution pH has strong impact for the coreactant pathway ECL²⁴. HEPES has two pKas on the two amine groups at 7.5 and 10 respectively. The near IR ECL signal is generated by oxidizing both AuNCs and the coreactant HEPES near electrode surface at appropriate electrode potentials. In the oxidation-reduction ECL pathway,²² one of the tertiary amine on HEPES is oxidized and subsequently undergoes deprotonation on a neighboring methylene group forming a highly reductive radical intermediate. The radical then reduces the oxidized AuNCs to form the excited species AuNC*. The AuNC* returns to the ground state by emitting photons which is collected by the camera as ECL signal.

Higher HEPES concentration, or more specifically more deprotonated nitrogen atom in tertiary amines with neighboring alkyl groups, will result in higher near IR ECL signal. Within each cycle when stepped to the oxidation potential, a strong ECL peak decays to a steady-state plateau over time. The decay profile is largely exponential which corresponds to the consumption of HEPES in the electrical double layer (EDL) of the electrode and the establishment of diffusion limited steady-state flux. In other words, both the ECL peak and the steady-state plateau at a given time after the application of oxidation potential should have the same dependence on the HEPES concentration. Correspondingly, the electrode potential is stepped periodically or cyclically to opposite polarity to refresh the concentration profiles in the electrode vicinity (double layer region). Because the ECL peak intensity is transient and the captured values are limited by the camera exposure time, plateau intensity is analyzed next as calibration profiles.

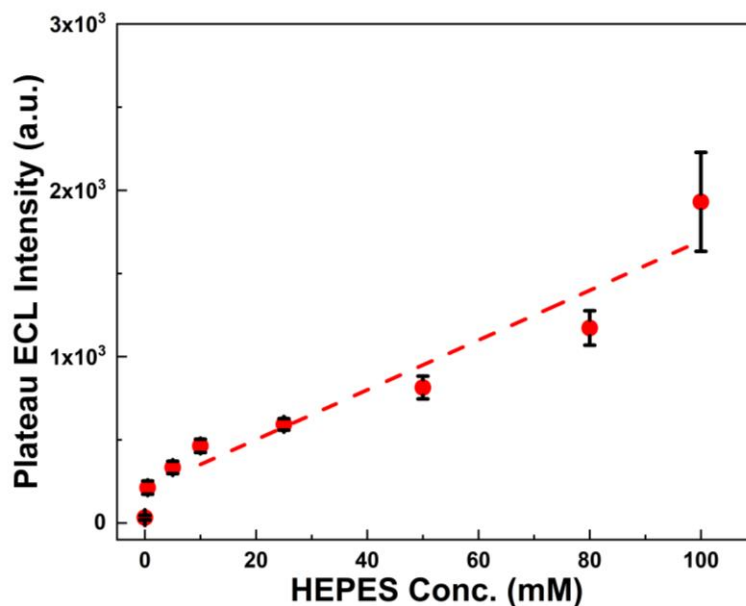


Figure 2.8 The near IR ECL signal dependence on HEPES concentration. The solution contains $50 \mu\text{M}$ Au-LA with 0.2 M NaClO_4 as supporting electrolyte. ECL intensity at 8 s was averaged over ten cycles at each concentration (data from Fig. 2.6). Error bar is the standard deviation of ten repeating measurement cycles. Dash line is a linear fitting in approximation.

The ECL signal particularly at steady state is highly consistent over repeated cycles. The steady state ECL intensity is plotted against the HEPES concentration in Fig 2.8. The ECL signal increases with the increment of HEPES concentration non-linearly over the whole tested concentration range. By analyzing the ECL noise level in Fig. 2.7 and under representative conditions, considering a qualitative lower detection limit at 3X signal/noise ratio, sub millimolar at the steady-state and much higher sensitivity based on ECL peak can be anticipated upon further development and optimization for a given analyte.

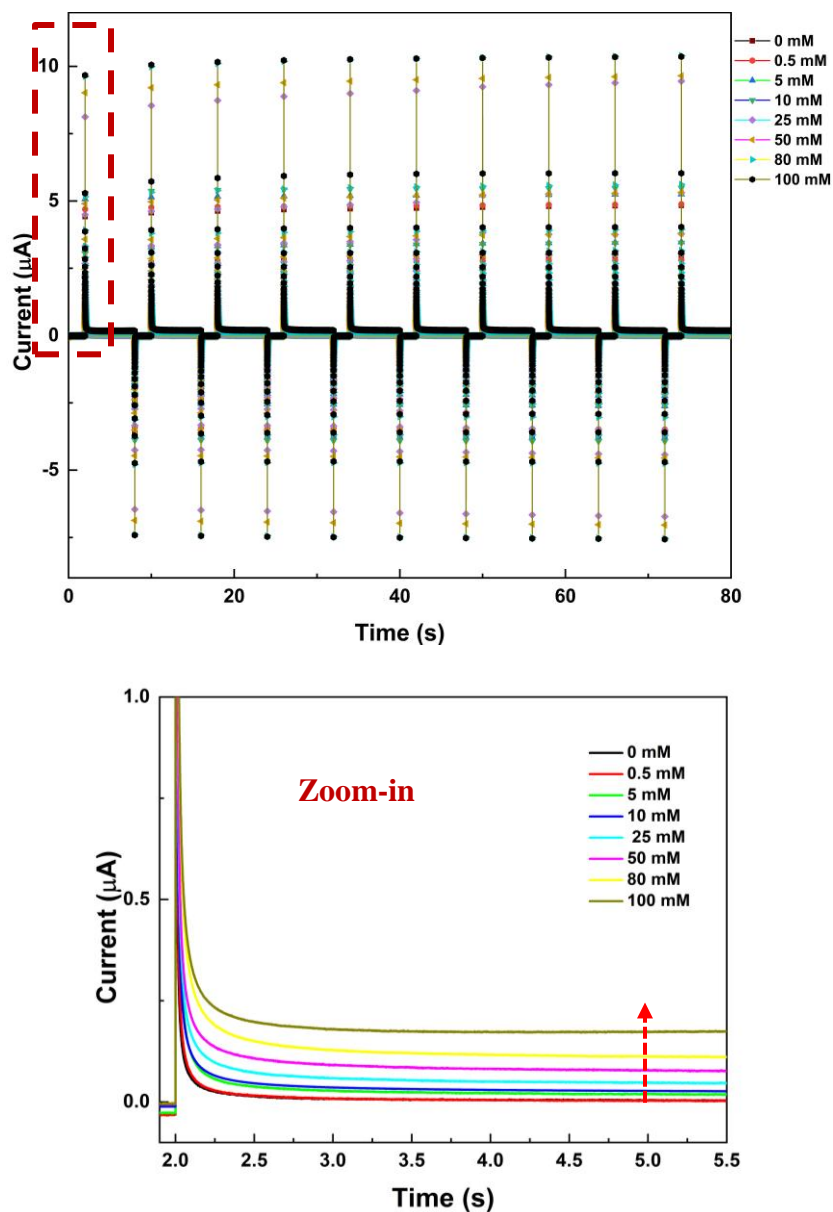


Figure 2.9 Current vs time profile for near IR ECL. The electrode potential was held for 2s at -0.8 V and then step to 1.2 V for 6 s for 10 cycles. The bottom panel zooms in the first cycle to illustrate the plateau current.

The current-time profiles in the corresponding ECL measurements are plotted in Fig. 2.9. The direct current-time profile is collected simultaneously with the near IR ECL signal. The steady-state or plateau current from the corresponding ECL measurements increases as HEPES concentration increases which matches the trend with the near IR ECL signal. The trend could be

observed under positive potential while HEPES being oxidized. There is no correlation nor increment for neither ECL or current signal under negative potential range. Because any potential steps will be associated with significant charging current due to EDL polarization, only steady-state current was analyzed next for the correlation with ECL signals.

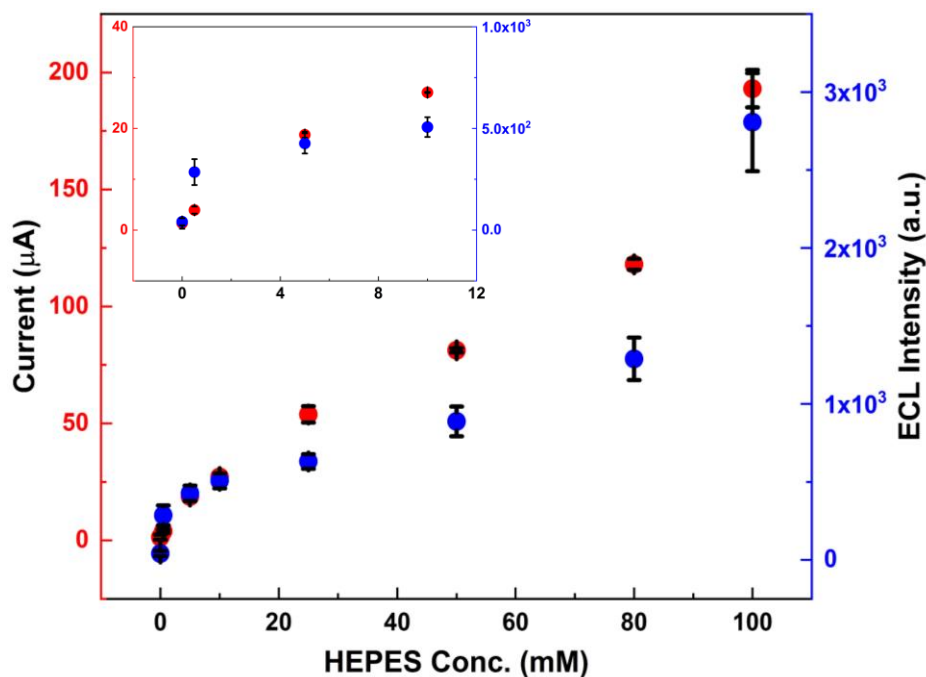


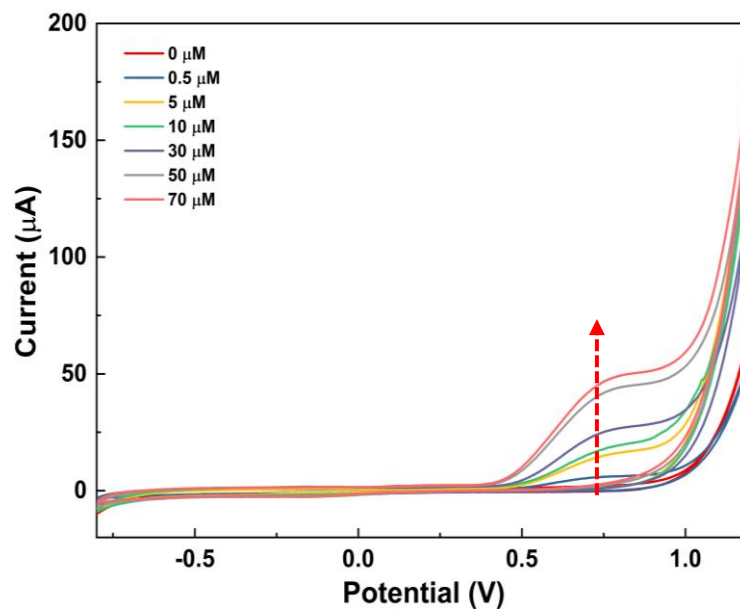
Figure 2.10 Correlation of the steady state ECL intensity and current at different HEPES concentrations. Error bar is the standard deviation. The current (red sphere) and ECL (blue square) signals are taken at the same time point, i.e. at 5th second then every 8 s (13th s, 21st s, 29th s, 37th s... data from Fig. 2.7 & Fig. 2.9).

Both current and ECL signals increase with HEPES concentrations following the same qualitative trend. While both signals are activated by the electrode oxidation, ECL generation requires additional charge transfer processes after the oxidized intermediates are produced, including proton/charge transfer, diffusional collision, and possible cyclic/catalytic reactions. Systematic study is needed to better understand different mechanisms and reaction processes. Because the two signals depend on different factors/processes that can be employed for cross-

checking, the calibration profiles of both current and ECL as dual signals will enable quantitative analysis of target analytes with greatly reduced false positive/negative responses.

2.4.3 Current and ECL responses by varying AuNCs concentration in fixed HEPES concentration

(A)



(B)

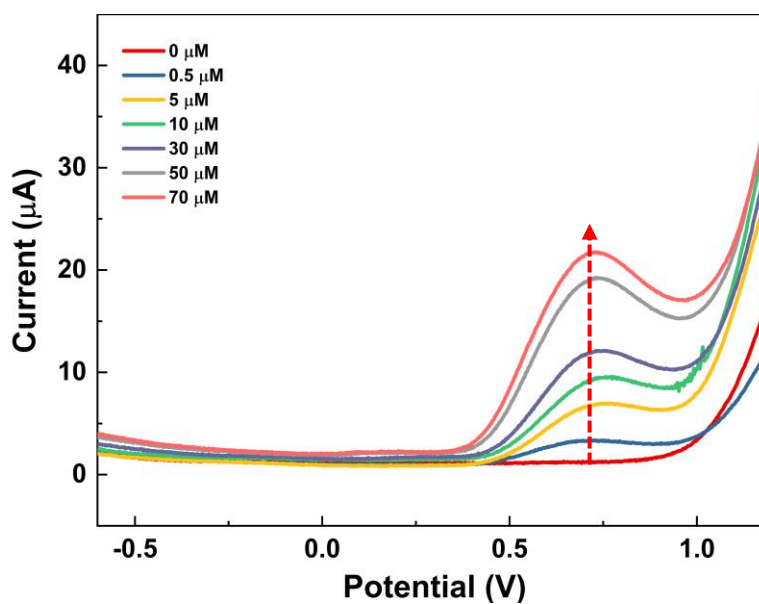


Figure 2.11 The dependence of anodic current on Au-LA concentration in (A) CV and (B) SWV. Data collected in 100 mM HEPES at pH 7.4 with 0.2 M NaClO₄. The CV scan rate was 0.1 V/s. The frequency 25 Hz, pulse size 25 mV and step size 2 mV were used in SWV.

The catalytic role of AuNCs in the oxidation of HEPES is further confirmed by the results in Fig. 2.11. With no Au-LA NCs in the solution, no anodic current or redox reactions can be observed in CV or SWV even if 100 mM HEPES is present other than the oxidation of solvent water beyond +1V. With sub- μ M Au-LA NCs added in the test solution, an anodic peak at around 0.75 V appears in both CV and SWV and peak current increases with the Au-LA NCs concentration. With the Au-LA NCs present despite the concentration much lower than HEPES, the oxidation peak at around 0.75 V with ITO electrode is close to the oxidation of HEPES on glassy carbon electrode (unpublished results).

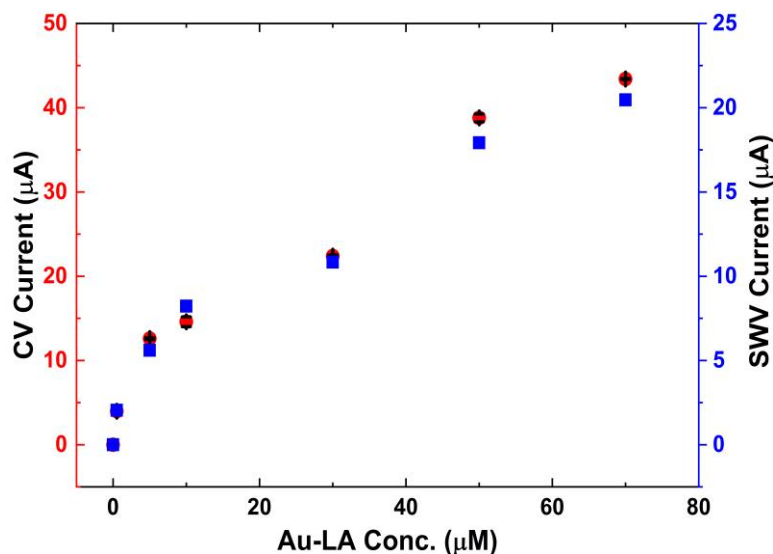


Figure 2.12 The dependence of current from CV and SWV on Au-LA NCs concentration. Current values were read at the peak around 0.75 V for each concentration in Fig. 2.11. Red spheres and blue squares are CV and SWV respectively.

The peak current analysis in Fig. 2.12 shows the same trend from SWV and CV of the current dependence on Au-LA NCs concentration. The higher the Au-LA NCs concentration in the solution, the higher the current signal is. Similar to the dependence on HEPES concentration,

the calibration profile is non-linear in the tested concentration range, likely due to the diffusion of both AuNCs and HEPES in solution. Again, CV provides diagnostic insights that the oxidation is irreversible while SWV offers better sensitivity by the subtraction of background charging current. From the data in Fig. 2.11 and the analysis in Fig. 2.12, it is obvious that nanomolar concentration of the AuNCs is already adequate to generate detectable current signals. The AuNCs concentration can be further lowered if needed.

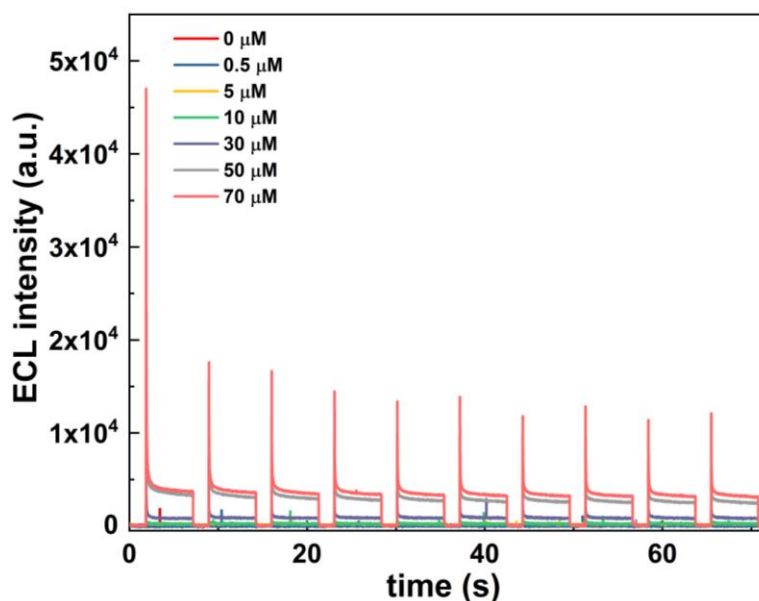


Figure 2.13 Near IR ECL signal at different AuLA NCs concentrations. The electrode potential was held for 2s at -0.8 V and then step to 1.2 V for 6 s over 10 repeated cycles.

HEPES itself at 100 mM concentration does not generate detectable ECL signal under comparable measurement parameters. When the potential is stepped to + 1.2 V, the overpotential is sufficient to drive anodic processes to oxidize both coreactant HEPES and Au₂₂-LA₁₂ at the ITO electrode surface and generate ECL through subsequent reactions between the two types of intermediates. In each potential step cycle, the ECL peaks drop immediately after the positive potential is applied followed by a gradual decay. The trend can be explained by the consumption

of reactant/s in the ECL and steady-state diffusional flux after the concentration gradient is gradually established.

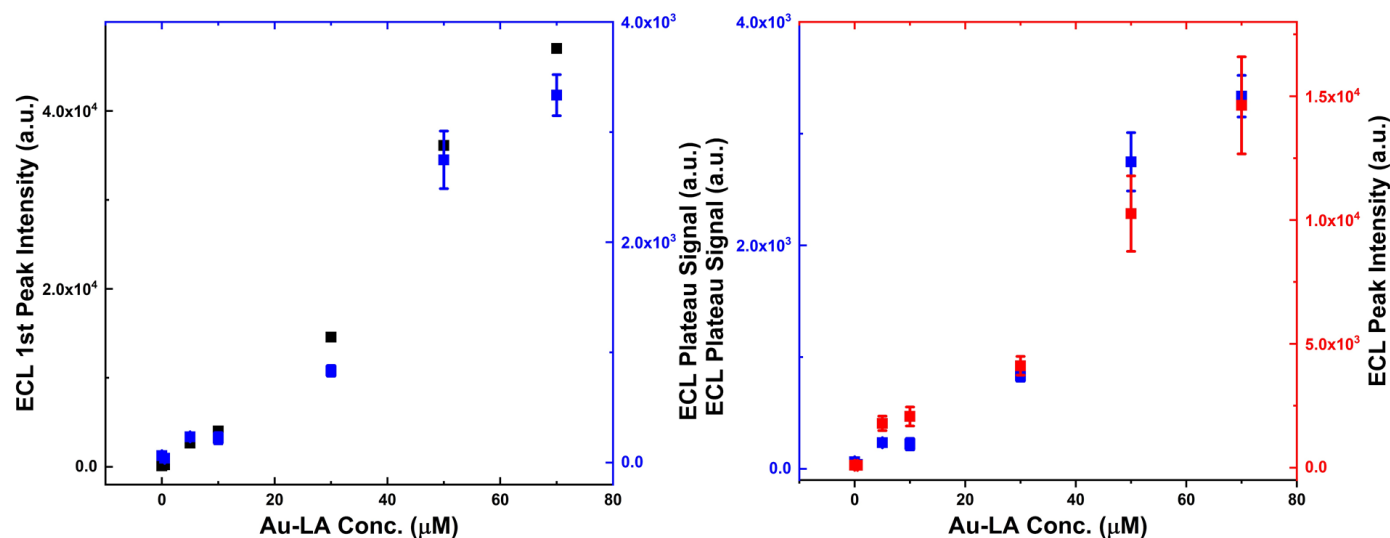


Figure 2.14 Analysis of ECL intensity (results in Fig. 2.13). The steady-state intensity at the plateau is averaged over ten cycles as reference. The left panel compare to the 1st peak, while the right panel compares to the average peak intensity of the following nine cycles. Linear fitting of all three data sets has an $R^2 > 0.9$.

The near IR ECL signal dependence on varying Au-LA concentration in 100 mM HEPES at pH 7.4 with 0.2 M NaClO₄ is showing in fig 2.14. The 1st peak signal verses concentration has linear fit $R^2 = 0.98$; the average peak intensity verses concentration has linear fit $R^2 = 0.92$, and the ECL plateau intensity taken at every 8th second verses concentration has linear fit $R^2 = 0.90$. The 1st ECL peak gives a much higher intensity then decay to steady-state ECL signal. With HEPES in high excess, pseudo first order dependence on the AuNCs is expected. The understanding is confirmed by the linear dependence of near IR ECL signal on Au-LA NCs concentration shown in Fig. 2.14. Accurate reading of the transient ECL peak intensity is limited by the camera exposure time at about 13.3 milliseconds. Though the ECL peak in the first cycle is consistently much stronger than the later cycles in repeated measurements, which is favorable for applications in the detection of low abundance analyte, rigorous validation and correlation to

more robust signals are necessary. The average plateau intensity at steady-states and the ECL peaks in later cycles are averaged for each concentration trace in Fig. 2.13. All three ECL intensity parameters display the same linear trend with decent fitting quality. Therefore, both ECL peak, steady-state, or integrated area if necessary, can be employed as signals for the detection in future applications.

2.4.4 Surface deposition of AuNCs film on ITO electrodes as integrated detection platform

When the Au-LA NCs are in solution, the NCs diffuse to and from the electrode surface then undergo redox reactions. For ECL generation, collisional reactions between the AuNCs and HEPES species at the electrode vicinity (EDL region) are needed within the lifetime of the radical intermediates after electrode reactions. Immobilization of the AuNCs on electrode surface will eliminate diffusion loss and could simplify the reaction pathways for better signal generation. Also, the ITO electrodes modified with Au-LA NCs film can be viewed as integrated sensor devices for the detection of drugs or biomarkers with appropriate tertiary amine structures.

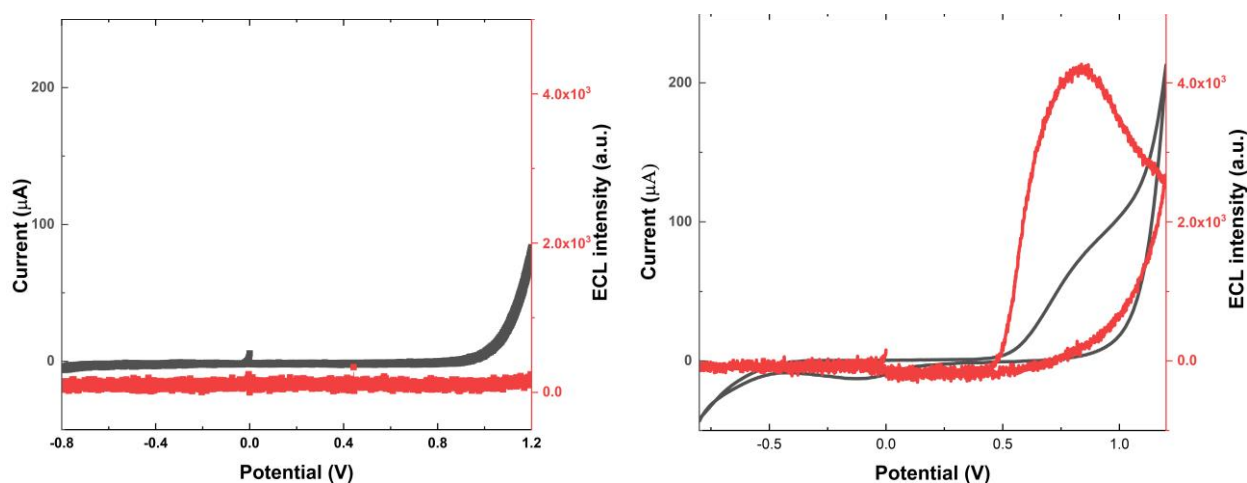


Figure 2.15 CV-ECL profiles of bare ITO (left) and ITO with Au-LA NCs film (right). Black curve is current from CV (left axis) and red is ECL intensity (right axis). Tested in 25 mM

HEPES with 0.2 M NaClO₄ solution at pH 7.4. The current and ECL scales are set the same in the two panels for direct comparison.

The results in Fig. 2.15 highlight the efficacy of AuNCs film on ITO in enabling both current and ECL signals in response to HEPES as prototype analyte. As expected, no redox reaction or ECL signal could be observed with bare ITO electrodes without Au-LA present. When the Au-LA NCs film on ITO, anodic current and ECL signal are generated and peaked at around 0.75 V. The CV-ECL features are qualitatively consistent with the solution results²⁸ which further supporting the catalytic effect of AuNCs on HEPES oxidation which enhances the ECL signal. . The cathodic current around 0 V corresponds to the reversal reduction, partial instead of complete based on the much weaker current amplitude. As a reminder, reversal reduction of those oxidation processes was not detected when the AuNCs are free diffusing in solution.

Uniform and stable surface films are non-trivial to fabricate. Because the current and ECL generation require efficient electron transfers through electrode surface, common strategies to stabilize surface films should be practiced with caution because additional materials layers could impede charge transfer or signal generation. To be more compatible with aqueous soluble Au-LA NCs, the ITO surface was treated to be more hydrophilic for improved affinity in aqueous environment. The treated ITO electrode was referred as 'bare ITO' for film deposition. It is worth mentioning that the surface treatment to lower the hydrophobicity of the ITO electrode does not impact the surface roughness or chemical composition of the ITO surface.¹⁸ The Au-LA NCs are poly anions with significant hydrophobic domains in ligand shell due to the molecular structure of lipoic acid ligands^{37, 41}. Coordination with multivalent cations or lower pH

will cause the precipitation of Au-LA NCs from solution²⁸. Next, surface deposition of Au-LA NCs as film on the ITO electrodes is achieved by gradual precipitation with Zn^{2+} .

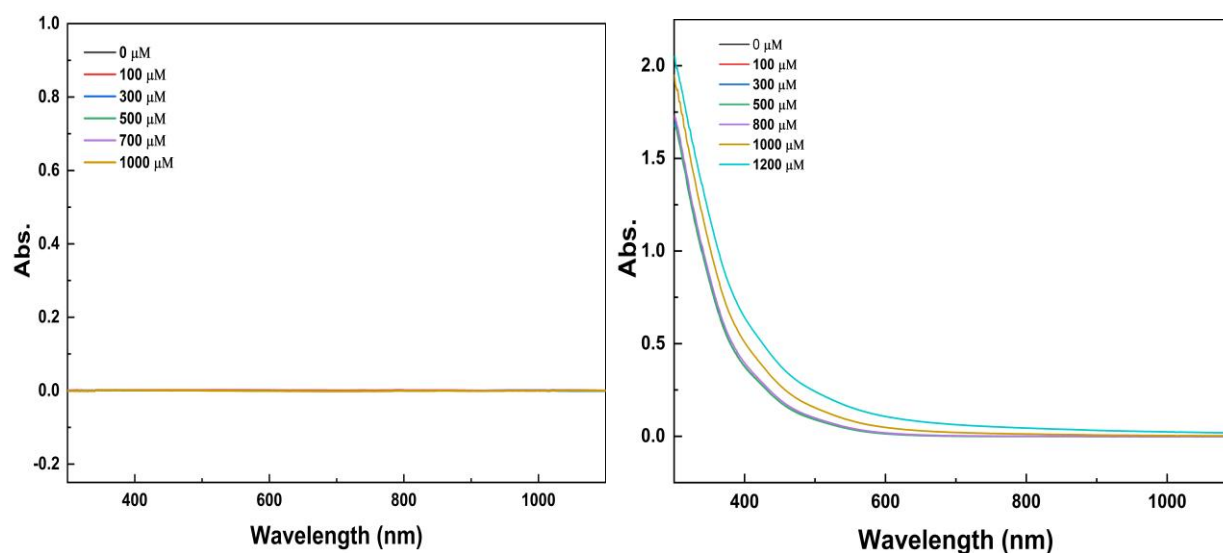


Figure 2.16 UV-Vis spectra of $ZnCl_2$ titration in 25 mM HEPES (left), 50 μM Au-LA in 25 mM HEPES (right) with 0.2 M $NaClO_4$

Titration of Zn^{2+} ions into Au-LA NCs-HEPES solution will cause precipitation when Zn^{2+} concentration is above ca. 1mM. Measured by the UV-vis spectroscopy, the spectrum shifts up as shown in Fig 2.16. The change indicates the formation of precipitants that scatters light. Over time, yellow precipitates become visible gradually in the AuNCs- Zn^{2+} -HEPES system measured in the right panel. Without AuNCs, no change in absorption spectrum is recorded (left) nor precipitates emerge. The precipitation can be understood from the combined effects of lower electrostatics repulsion, hydrophobic interactions of ligands, and entropy gain through crosslinking/multi-valent coordination. There are about 12 lipoic acid ligands per Au_{22} NCs²⁷. The Zn^{2+} ion could serve as counter ions for two carboxyl groups, either within a single NC or crosslink two NCs. Meanwhile, at pH 7.4, one of the amine group on HEPES is about half deprotonated²⁸. The lone pair of the nitrogen could weakly coordinate with metal ions. For

comparison, metal ions with lower binding affinity, such as Mg^{2+} and Ca^{2+} studied previously in the group, precipitation is far less effective and not used in this project²⁸.

ITO electrodes are generally soaked in the solution mixture over a certain incubation period during which the yellow precipitates are slowly deposited on the hydrophilic ITO surface to form a thin layer or film. At the end of the incubation, the ITO electrode is slowly pulled out of the solution and air dried prior to the following electrochemical measurements.

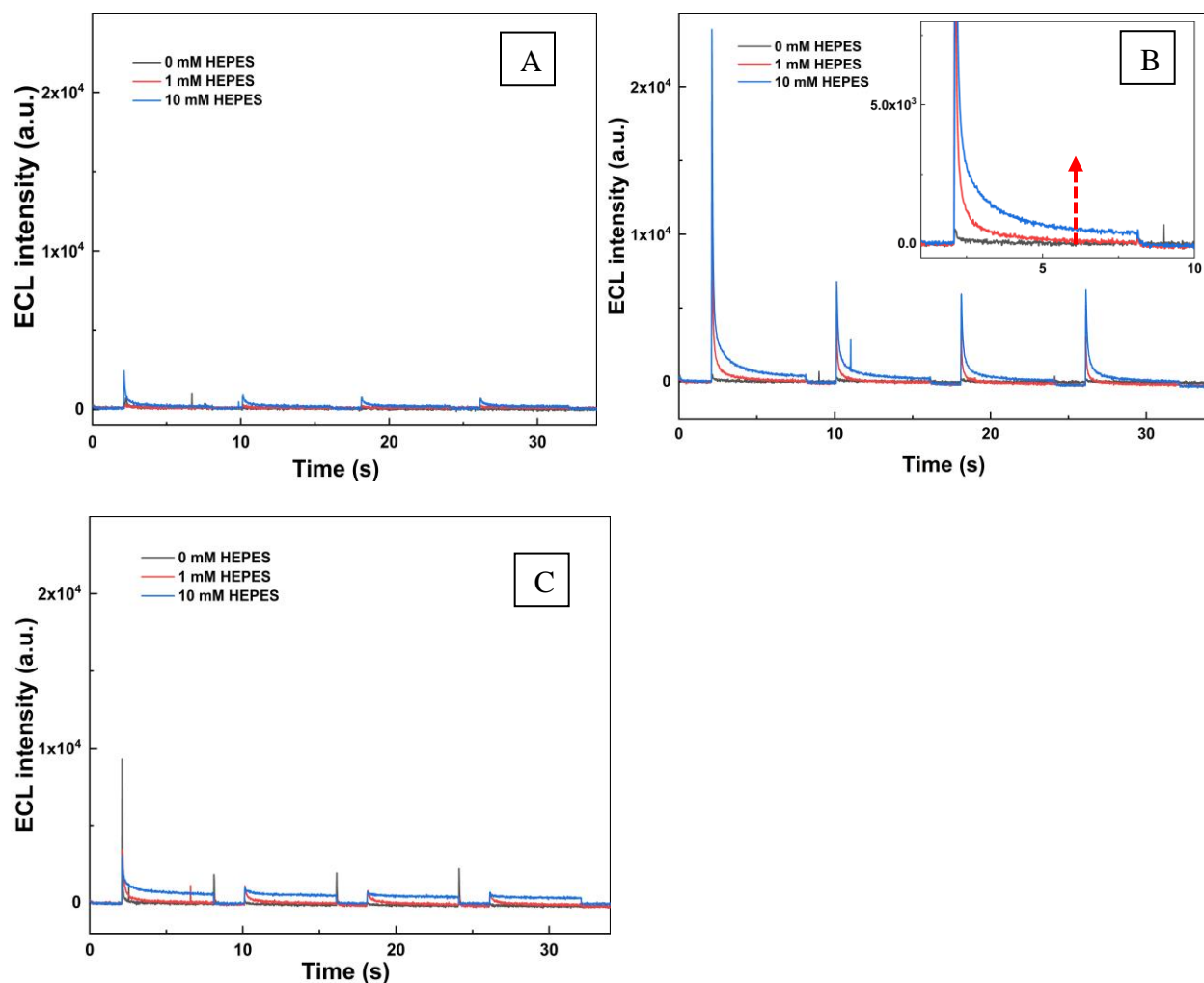


Figure 2.17 ECL characterization of AuNCs film deposited over different incubation period of (A) 30 mins (B) 2 hours with first cycle zoom-in (C) 12 hours. The ITO electrodes were soaked in 1 mM $ZnCl_2$ with 50 μM Au-LA and 25 mM HEPES for AuNC film preparation. The ECL was measured in different HEPES solutions containing 0.2 M $NaClO_4$ as supporting electrolytes and 1 mM $ZnCl_2$ to suppress film dissolution. The electrode potential was held for 2s

at -0.8 V and then step to $+1.2$ V for 6 s for 4 cycles. Measured under ambient condition without degas.

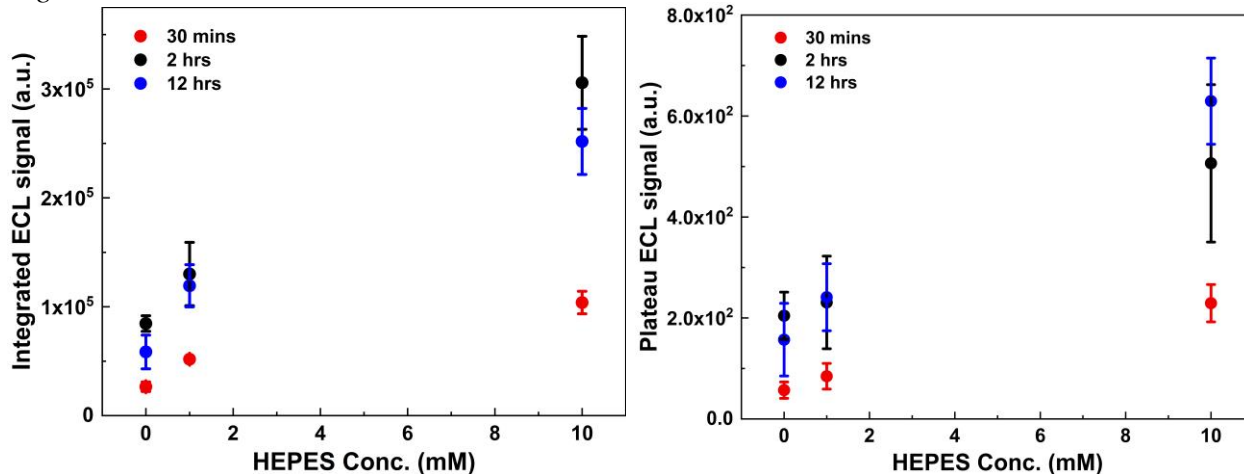


Figure 2.18 Analysis of ECL performance of different AuNCs films in representative HEPES concentrations from data in Fig. 2.17. The integrated ECL signal (left) was calculated from the sum area of the ECL intensity in one cycle. The ECL signal at steady state (right) was from data at 3s after $+1.2$ V was applied. The symbol and error bar are the mean and standard deviation from the four repeated cycles in each measurement.

The incubation time for the AuNCs film preparation is studied shown in Figure 2.17 and analyzed in Figure 2.18. The differences between 30 mins of incubation and longer time is obvious, meanwhile the difference between 2 hours and 12 hours incubation is hardly identifiable. Therefore, the 2-hour incubation is sufficient to make the ITO film using the selected deposition solution conditions and adopted in later studies. The AuNCs film modified ITO electrodes produce consistent ECL responses in repeated measurements in different HEPES concentrations. Without HEPES in the test solution as coreactants, however, the ECL signal is much weaker or insignificant. Both the integrated ECL signal and steady state signal increase with the HEPES concentration (linearly). The ITO film is treated with RCA-1 treatment^{14, 18} to increase the coverage of hydroxyl group on the surface before incubation. The film could be a very thin, spotty layer for 30 mins of the incubation, with time period increasing, more Au₂₂-

LA₁₂ cluster in the solution is able to attach to the hydrophilic ITO surface to form a more uniformed film layer.

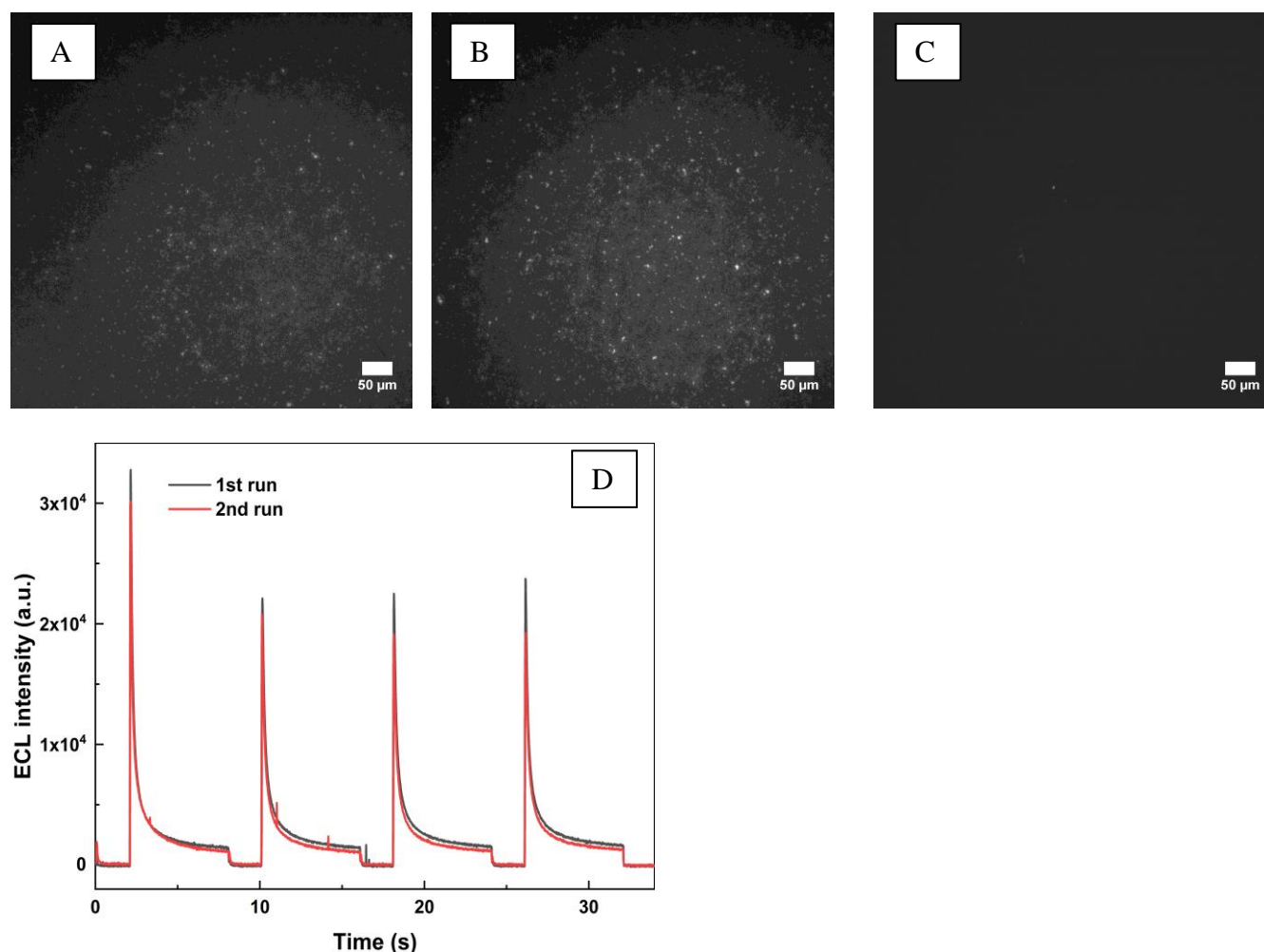


Figure 2.19 fluorescence microscopic imaging and stability of AuNCs film on ITO electrodes: (A) after 2-hour incubation/deposition; (B) after ECL measurements in 25 mM HEPES with 1 mM ZnCl₂ (C) after ECL measurements in 25 mM HEPES without ZnCl₂. The brightness and contrast of the images were set consistently for direct comparison. (D) The step ECL profiles of film stability in 1 mM ZnCl₂ with 25 mM HEPES. The electrode potential was held for 2s at -0.8 V and then step to 1.2 V for 6 s for 4 cycles. Measured under ambient condition without degas.

The signal stability and consistency are very important factors for sensor manufacturing. The stability of the AuNCs film on ITO electrodes is characterized by photoluminescence microscope imaging in addition to the near IR ECL tests. Near IR photoluminescence of AuNCs have been widely studied, but to a much less extent on solid surface as films⁴². The bright spots

in Figure 2.19 are the emission from the AuNCs aggregates. Note we are interested in make sub or few layers instead of thick films to have the contrast for mechanistic understanding with respect to the surface homo/heterogeneity. Before and after the electrochemical measurements with 1 mM ZnCl_2 present in the test solution, the emission features did not change by the qualitative comparison of image (A) and (B). In comparison, the bright emission is gone after the ECL tests without zinc ions confirmed in image (C). The Zn^{2+} ions play a very important role to suppress the dissolution of surface deposited AuNCs for better sensor stability. This is the same principle in the precipitation of AuNCs by Zn^{2+} in the film preparation. The stability of the surface deposited AuNCs film on ITO is also confirmed by the consistent near IR ECL profile after multiple cycles of measurements in 1 mM ZnCl_2 with 25 mM HEPES solution. Without the Zn^{2+} present in the testing solution, ECL signals diminish quickly (not shown).

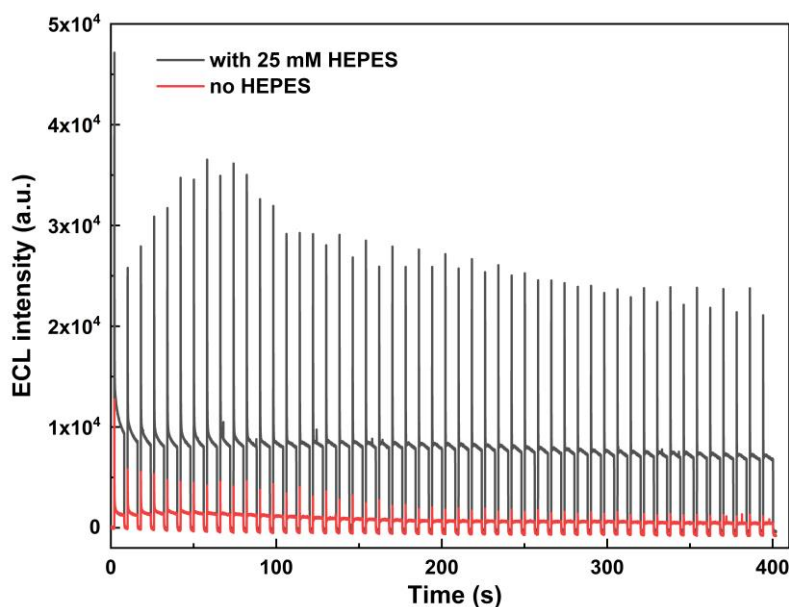


Figure 2.20 ECL signals from AuNCs film drop cast on ITO electrode tested in 0.2 M NaClO_4 electrolyte only (red, bottom curve) and 25 mM HEPES with 0.2 M NaClO_4 electrolyte (black, top curve). A 10 μL precipitating solution containing 50 μM Au-LA and 2mM ZnCl_2 with 25 mM HEPES was dropcast on ITO and air dried. The electrode potential was held for 2s at -0.8 V and then step to 1.2 V for 6 s for 50 cycles. Measured under ambient condition without degas.

As proof of principles for future practical applications, thicker films are prepared through drop cast and tested. The near IR ECL results are plotted in Figure 2.20. The thick film of AuNCs can be directly visualized displaying inhomogeneous surface patterns (dry spots). With more AuNCs available on electrode surface, long lasting and very strong near IR ECL signal can be detected. The ECL from the AuNCs film itself without HEPES in solution is likely resulted from the excess HEPES introduced during the drop cast process. Regardless, significant enhancement in the near IR ECL by HEPES is detected with highly reproducible and consistent signals prior to any optimization. It is anticipated that by better understanding in the reaction mechanism with thin films, and after the optimization of surface film preparation, robust sensor devices can be developed with dual modal current and near IR ECL signals that can be tailored for different drugs or biomarkers with suitable molecular structures and properties.

2.5 Conclusion

Signal-on detection strategy is developed based on aqueous soluble Au nanoclusters using optically transparent ITO electrodes and prototype analyte HEPES. Anodic current and oxidative-reduction ECL in near IR are demonstrated to be dual signals for improved specificity. The functions of the AuNCs are studied in two systems: free diffusing in solution and deposited on ITO as solid films. Lipoic acid stabilized Au₂₂ nanoclusters are found to effectively catalyze the oxidation of HEPES on ITO electrode. The anodic current signal in both CV and SWV can only be detected with the presence of AuNCs within the applicable potential range. Meanwhile, the near IR ECL signal from the AuNCs is enhanced by the oxidized tertiary amines in HEPES through coreactant pathway. Calibration profiles for both HEPES and AuNCs reveal nonlinear dependence on either concentration. As low as nanomolar concentration AuNCs are adequate to

catalyze the oxidation for signal generation. The relative complex reactions involving multi-species diffusion in solution is mitigated by the immobilization of AuNCs on ITO surface. Surface deposition of AuNCs is achieved by either incubation or drop casting a slow precipitating AuNCs solution. The conditions including the surface treatment of ITO, composition and kinetics of precipitation-incubation, and film stability in testing solutions are explored. The uniformness and stability of the AuNCs film are also surveyed by the imaging based on the photoluminescence of AuNCs. ECL from AuNCs films prepared under varied conditions are compared by testing in different HEPES concentrations. Thin films fabricated via incubation-precipitation are more uniform for mechanistic studies, while thick films from direct drop casting produce strong and long-lasting signals. Further basic study and parameter optimization could establish robust sensor devices for the detection of drugs and biomarkers with suitable tertiary amine molecular structures and redox properties.

3 SURFACE ASSEMBLY OF Au₁₂Ag₁₃ BIMETALLIC NANOCCLUSERS ON ITO ELECTRODES: NEAR IR ELECTROCHEMILUMINESCENCE AND OPTICAL IMAGING

3.1 Abstract

The rod-shape bimetallic Au₁₂Ag₁₃ nanoclusters (NC) is organic soluble with a ca. 40% quantum efficiency of near IR photoluminescence and displays record high near IR ECL in solution measurements.⁴³ In this chapter, the Au₁₂Ag₁₃ NCs are assembled on ITO electrode surface as potential integrated sensing devices. The NCs and the surface assemblies are insoluble in aqueous environment and thus function as more stable films for future analysis applications of suitable drugs or biomarkers. The NCs film with distinctly different morphologies were fabricated with different methods and under systematically varied conditions. Stable and uniform NCs films on ITO were obtained controllably and reproducibly by spin coating after optimization. Characterizations were performed by optical imaging and electrochemical methods. With the addition of tertiary amine drug cetirizine, the ECL signal increased drastically through coreactant oxidative-reduction pathway. The design principle is applicable to other organic soluble metal nanoclusters with well-established structures and properties for sensor development and applications.

3.2 Background and Strategy

The Ag₁₃Au₁₂ nanoclusters (NCs) exhibit high quantum yield (40%) in near IR photoluminescence⁴⁴. The energetics also enables hundreds-fold stronger near IR ECL than

Ru(bpy)₃ standard under coreactant oxidative reduction pathway⁴³. Like most other organic soluble metal NCs with beautiful atomic composition and structures elucidated, biomedical or analytical applications are basically infeasible due to the incompatibility with aqueous environment despite their rich optical and electrochemical properties. The impressive record-breaking near IR luminescent property of this bimetallic NC motivate us to exploring surface assembly strategies for analytical sensing applications. The bimetallic (AgAu)₂₅ cluster was synthesized by reacting a precursor Au₂₅(PPh₃)₁₀(SC₂H₄Ph)₅Cl₂]²⁺ cluster with doped Ag gives the rod-shape [Ag_xAu_{25-x}(PPh₃)₁₀(SC₂H₄Ph)₅Cl₂]²⁺ (x ≤ 13)⁴⁴ nanocluster⁴⁴.

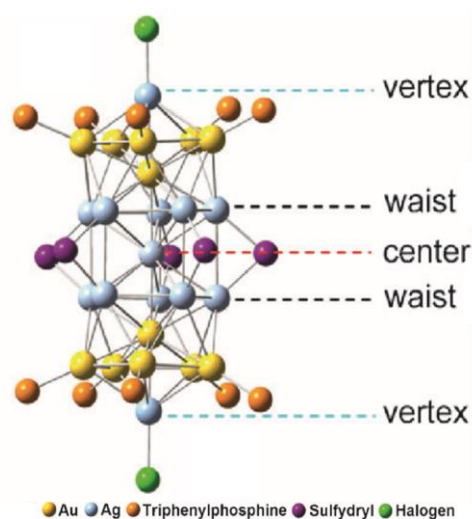


Figure 3.1 X-ray structure of rod-shape Ag₁₃Au₁₂ nanoclusters (NCs)⁴⁴

As reported, when the Ag doping x=13, the near IR photoluminescence and the QE reaches the highest value⁴⁴. The atomic structure shown in Figure 3.1 is resolved by X-ray crystallography analysis of single crystals of this Ag₁₃Au₁₂. A stock solution of Ag₁₃Au₁₂ NCs dissolved in organic solvent dichloromethane (DCM) was used for surface film preparation. The Ag₁₃Au₁₂ NCs film on ITO electrode is insoluble in the aqueous solution and thus intrinsic stable for analysis applications in for example biological samples at physiological pH. The ECL, photoluminescence and absorption spectra of the Ag₁₃Au₁₂ NCs in solution are provided in Figure 3.2 for reference.

The near IR photoluminescence displays an emission maximum at around 760 nm after excited with 365 nm wavelength. The UV-visible absorbance and luminescence intensity are convenient features to characterize the concentration/amount of the NCs in solution and on surface.

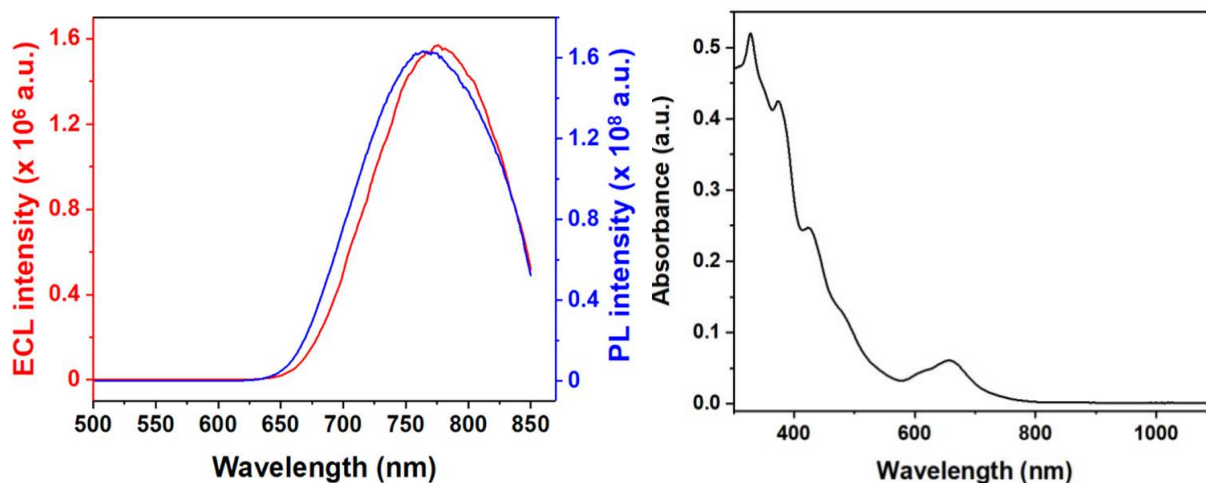


Figure 3.2 Spectroscopic features of $Au_{12}Ag_{13}$ in solution: ECL and PL spectra (left) and UV-vis absorption spectrum (right). The ECL spectrum was collected with $10 \mu M Au_{12}Ag_{13}$ and $1 mM TPrA$ under $+1.0 V$. The PL nanocluster sample is about 10 times less concentrated without $TPrA$. The PL spectrum profile was corrected. (Take from ref. ⁴³)

In this study, ITO slides are used as working electrode because of its optical transparency and electrical conductivity. Different method was attempted to fabricate controlled surface assembly structures or uniformed films of $Au_{12}Ag_{13}$ NCs on the ITO glass. The NCs on ITO are characterized by optical imaging and electrochemical measurements. Rather than using chelator EDTA or pH buffer HEPES as tertiary amine coreactants as in our previous reports^{27, 28}, the enhancement in near IR ECL signal was demonstrated with tertiary amine containing drug cetirizine as coreactant.

The compound cetirizine dihydrochloride, commonly referred to as cetirizine hydrochloride or cetirizine HCl, is the active ingredients of commercial drug Zyrtec. Zyrtec was approved by FDA (U.S. Food and Drug Administration) as prescription in 1995, then approved

for OTC (over-the counter) drug in 2007.⁴⁵ It is a non-drowsy antihistamine that temporarily relieves the symptoms like itching, swelling eyes, runny nose and sneezing from respiratory allergies or hay fever, also significantly reduces uncomplicated skin pruritus from insect bites. Zyrtec contains 10 mg of cetirizine HCl in each tablet; the molecular formula is $C_{21}H_{25}ClN_2O_3 \cdot HCl$ with molecular weight 461.82 g/mol, the chemical structure is provided in Figure 3.3. One of the tertiary amine groups has a pKa around 8, the other amine group closer to the aromatic groups has the pKa of 2.2, and the carboxyl group has the pKa at 2.9.⁴⁵⁻⁴⁷ At physiological pH 7.4, the amine group with pKa 2.2 is fully deprotonated and the other one is partially deprotonated. Cetirizine is used as a prototype for future tertiary amine drug sensing development due to its easy accessibility and low cost.

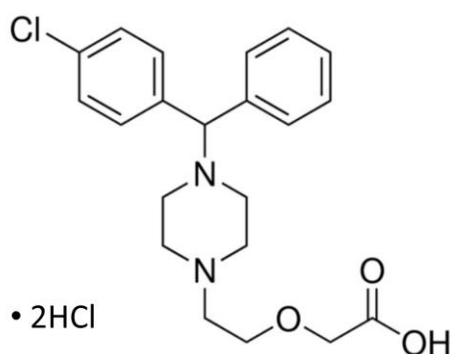


Figure 3.3 Cetirizine dihydrochloride structure

3.3 Experimental Details

3.3.1 Materials

[2-[4-[(4-Chlorophenyl) phenylmethyl]-1-piperazinyl] ethoxy] acetic acid dihydrochloride (Cetirizine, $\geq 98\%$), sodium perchlorate hydrate ($NaClO_4 \cdot xH_2O$, $\geq 99.99\%$), Sodium phosphate monobasic monohydrate ($NaH_2PO_4 \cdot H_2O$, $\geq 98\%$), Sodium phosphate dibasic heptahydrate ($NaH_2PO_4 \cdot 7H_2O$, $\geq 98\%$), Chloroform ($CHCl_3$, $\geq 99.8\%$), were purchased from Sigma-Aldrich and used as received. Methylene Chloride or dichloromethane (CH_2Cl_2 , HPLC

grade), Acetonitrile (CH₃CN, HPLC grade) purchased from Fisher chemical and dried before used. Rod-shape [Ag_xAu_{25-x}(PPh₃)₁₀(SC₂H₄Ph)₅Cl₂]²⁺ (x ≤ 13) NCs was provided by Dr. Manzhou Zhu's group⁴⁴. In all aqueous solution preparations, nanopure water (>18 MΩcm) from a Barnstead system was used.

3.3.2 ITO electrode preparation

Corning alkaline earth boro-aluminosilicate glasses coated with indium tin oxide (ITO) were used as electrodes. The ITO electrodes were purchased from Delta Technologies (CB-40IN), R_s = 4-10 Ω. The as prepared ITO surface is relatively hydrophobic that is readily compatible with organic soluble NCs. The ITO electrode was first cleaned with a general cleaning process by ultrasonicing in nanopure water, ethanol and nanopure water (1:3), and nanopure water for at least 15 minutes each before use.

3.3.3 Electrochemical measurements

Cyclic voltammograms were collected using a potentiostat (Gamry Reference 600) with the sample in a Faraday Cage. A three-electrode setup uses an Ag/AgCl wire as a quasi-reference electrode, platinum (Pt) foil as a counter electrode and ITO as a working electrode. Phosphate Buffered saline (PBS) pH 7.4 was used to prepare cetirizine solutions and as controls. Scan rate was 0.1 V/s in all CV measurements.

3.3.4 Near IR Electrogenerated chemiluminescence measurements

The ECL was measured in a quartz cuvette (Figure 2.2). A 3-D printed spectrometer cuvette holder was used to hold the cuvette in front of the camera window at a fixed position. An ITO electrode is fixed with a cap on the top of the cuvette to ensure consistent electrode-camera alignment. For results to be directly relevant to real life application settings, all measurements

were performed under ambient conditions without degassing. Unless defined otherwise, the electrode potential was held for 2s at -0.8 V and then stepped to 1.2 V for 6 s. The emission intensity was recorded with an Andor iDUS CCD camera (Model DU401A-BR-DD). To synchronize the camera response and the electrochemical measurements, the camera is externally triggered by the potentiostat (Gamry Reference 600) at time zero when the potential is applied. The ECL intensity is the sum of photon counts from all pixels; the exposure time is 15 ms for step ECL measurement unless otherwise noted.

3.3.5 Microscopy imaging

A fluorescence microscope (Olympus IX73) was used for the imaging of metal NCs on ITO. An 377 \pm 50 nm excitation filter and 647 nm long pass emission filter were used to record photoluminescence with 33 ms exposure time. The excitation light source is a high-power LED light (Excelitas Technology, X-Cite 120 LED Boost).

3.3.6 Dip coating method

Dip coating method constitutes a simplified Langmuir-Blodgett type surface film preparation. A stock solution of Au₁₂Ag₁₃ NCs dissolved in DCM (absorbance at 360 nm is 0.6 measured with a 1 cm light path) was further diluted into different concentrations as deposition solutions.⁴⁴ After an ITO electrode (around 1 cm in length) is vertically immersed in the deposition solution, the ITO was manually pulled out at a constant speed (around 1 mm/s) and then the extra solution accumulated at the bottom was removed by tapping on a filter paper.

3.3.7 Spin coating method

Three types of Au₁₂Ag₁₃ NCs solution were spin coated to fabricate NCs film on ITO electrodes with a spin coater (Chemat Technology series KW-4A) with 1.0 CG aluminum vacuum chuck under vacuum condition. The first is the stock solution in pure DCM with the

absorbance at 360 nm at about 0.6 measured with a 1 cm light path. The spin speed was 600 RPM and the time of spin is set to 1 min with dynamic dispense. A 5 μ L drop of the NCs solution was applied either 10 times or 25 times during the dynamic spinning to deposit different amount of NCs. The second is a 1:1 volume ratio of the stock DCM solution and ACN mixture, and the third solution is a 1:1 volume ratio of stock DCM solution with chloroform mixture. Dilution with either ACN or chloroform were made to slow down the evaporation rate for a more uniformed film deposition. During the dynamic spin, the speed is 900 RPM, and the duration is 1 minute.

3.4 Results and Discussion

3.4.1 Au₁₂Ag₁₃ nanocluster modified ITO electrode surface

The goal of this project is to achieve controlled surface distribution and coverage of NCs. Different surface assembly methods are explored accordingly. A widely distributed and low surface coverage will be of fundamental interest toward single molecule type studies, in which the signal will be low. A high surface coverage and uniform film will be suitable to generate strong and consistent signals for detection applications.

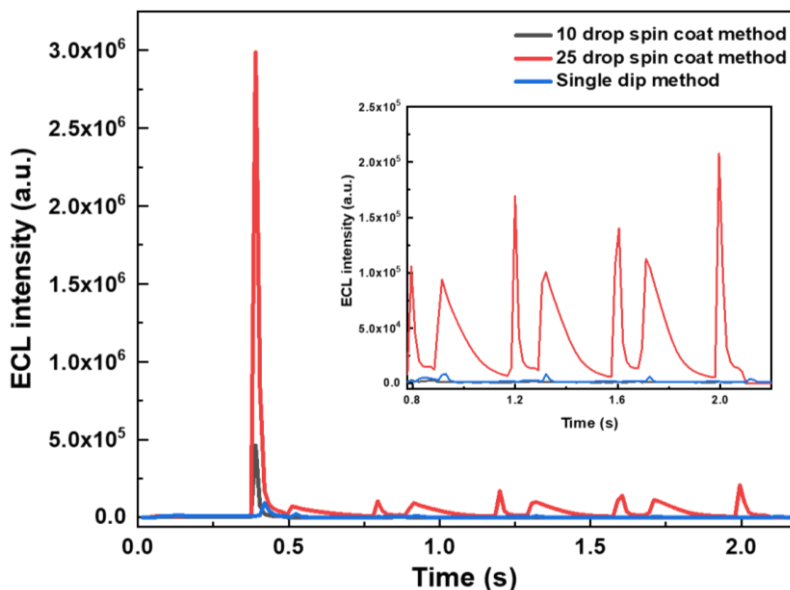


Figure 3.4 . The step ECL signals from different surface deposition methods. The stock NCs DCM solution was used in all three preparations. Tested in PBS buffer at pH 7.4. The electrode potential was held for 0.3s at -1.0 V and then stepped to 1.0 V for 0.1s. No potential was applied after 2.3s. Inset better illustrates the low intensity signals (first cycle excluded).

The assembly of organic soluble NCs on the electrode surface make them compatible and applicable to applications in aqueous environment. The elimination of the diffusion process involving NCs could also simplify the mechanism and improve the enhancement of near IR ECL and current signals by target analytes such as piperazine drugs. ECL responses from surface assembled NCs prepared with different methods are compared in Figure 3.4. Though very preliminary, it can be semi-quantitatively concluded that more materials, i.e. 25 drops over 10 drops in spin coating, generate stronger ECL signals (about 10 folds stronger). Both spin coating preparations produce much stronger ECL signal compare to the dip coating method. Without coreactants in the test solution, the ECL signal generates from self-annihilation pathway, i.e. both oxidized and reduced NCs are needed to generate the ECL signal. The ECL signal is therefore the strongest when the positive/negative potentials were stepped which decays quickly with each potential step. More specifically, a single oxidation or reduction potential would not

generate ECL, as is the case from zero to 0.3 seconds in the first step. Pre-existing reduced/oxidized NCs are necessary (via electrode reduction/oxidation) to react with the oxidized/reduced NCs produced by the newly applied potential. The first potential always generates much stronger ECL compared to later cycles regardless the surface preparation methods. Degradation of NCs and irreversible changes of surface assembly structures are among possible speculated reasons that require further study.

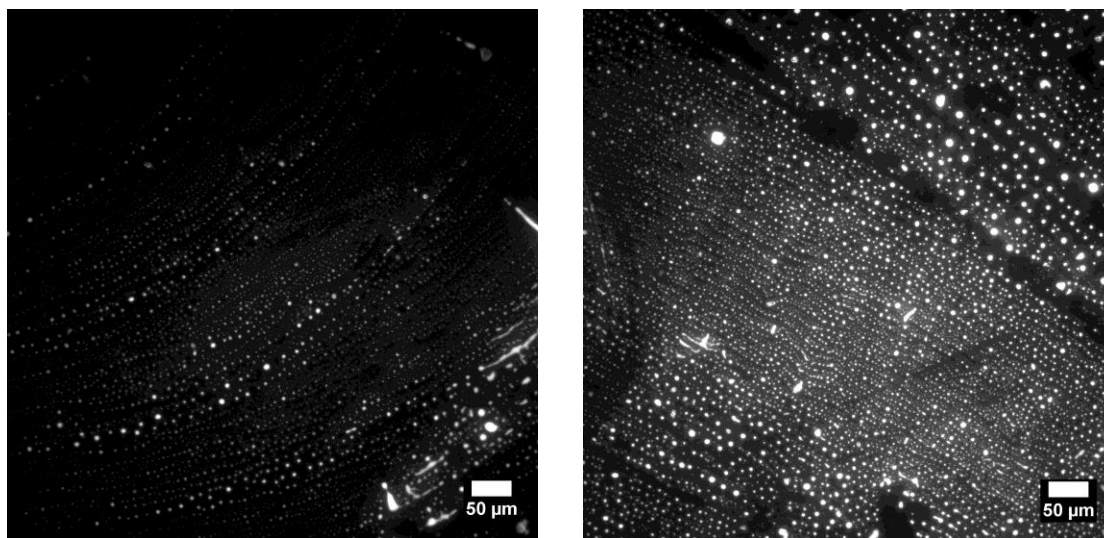


Figure 3.5 fluorescence microscopic imaging of surface deposited NCs by spin coating (left) 10 drops and (right) 25 drops of 5 μ L stock DCM solution. Spin coating speed was 600 RPM. Near IR photoluminescence from the NCs using 377 \pm 50 nm excitation filter and 647 nm long pass emission filter pass filter and a 40X objective. The contrast/brightness is set the same for all images.

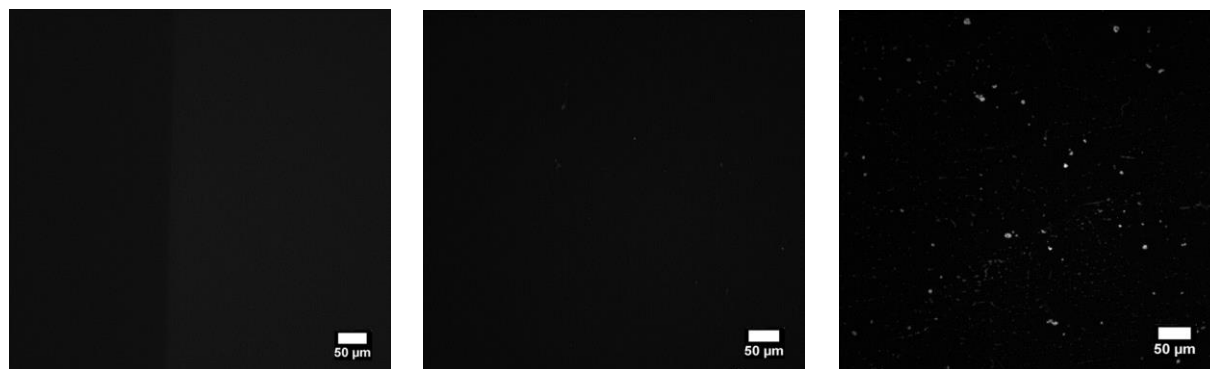


Figure 3.6 Fluorescence imaging of (left) Bare ITO surface (middle) Dip coating with instant dipping (right) Dip coating with 5 minutes incubation. Bright features are the near IR photoluminescence from the NCs. Images recorded using 377+/-50 nm excitation filter and 647 nm long pass emission filter and a 40X objective. The contrast/brightness is set the same for all images.

The surface NCs deposited under different conditions are directly characterized with microscope imaging of the near IR photoluminescence from the NCs in Figure 3.5 and Figure 3.6. The spin coating method with multi-drops of sample applied during spinning process deposits more material on the ITO surface. The aligned bright spots results from the fast evaporation of solvent DCM during the spinning. Similar features are observed throughout the ITO surface away from the center spot where the drops are added (not shown). The dip coating method is ineffective to deposit a large amount of NCs on the ITO electrode surface, particularly with less incubation time. With 5 minutes incubation in the dip-pull procedure, the overall surface coverage increased but the distribution is still not uniform. Overall, from both the ECL and photoluminescence imaging results, the spin coating method deposited more NCs with better surface coverage on the ITO electrode surface.

The consistent aggregate spots evenly distributed on ITO surface suggest that by fine tuning the solvent evaporation rate and spin speed, and with an appropriate affinity difference between the ITO surface and solvent with the NCs, more uniform surface distributions or films can be obtained. DCM has a low boiling point around 40 °C and thus fast evaporation rate which makes slower surface preparations, generally more favorable to prepare more uniform surface films, technically difficult. Multiple drop addition and relative slow spin speed, and longer incubation time, were adopted to extend the sample-surface interaction time. Other solvents such as ACN (boiling point 82 °C) and chloroform (boiling point 60 °C) are introduced in later studies. In addition to lower evaporation rates, the poorer solvent for the bimetallic NCs should

also increase the NCs' affinity/interaction with ITO surface and self-assembly processes relative to DCM.

3.4.2 The enhancement of surface near IR ECL signal by tertiary amine containing drug cetirizine

The near IR ECL of Au₁₂Ag₁₃ NCs generated through solution diffusion processes, via self-annihilation and coreactant pathways, has been reported by our group recently.⁴³ Notably, with prototype coreactant TPrA, the ECL signal was 400-folds stronger than that of Ru(bpy)₃ standard under comparable conditions. Next, the ECL from integrated NCs-ITO electrode device is studied in the presence of piperazine drug cetirizine which contains appropriate tertiary amine structures as coreactants to enhance the near IR ECL signal.

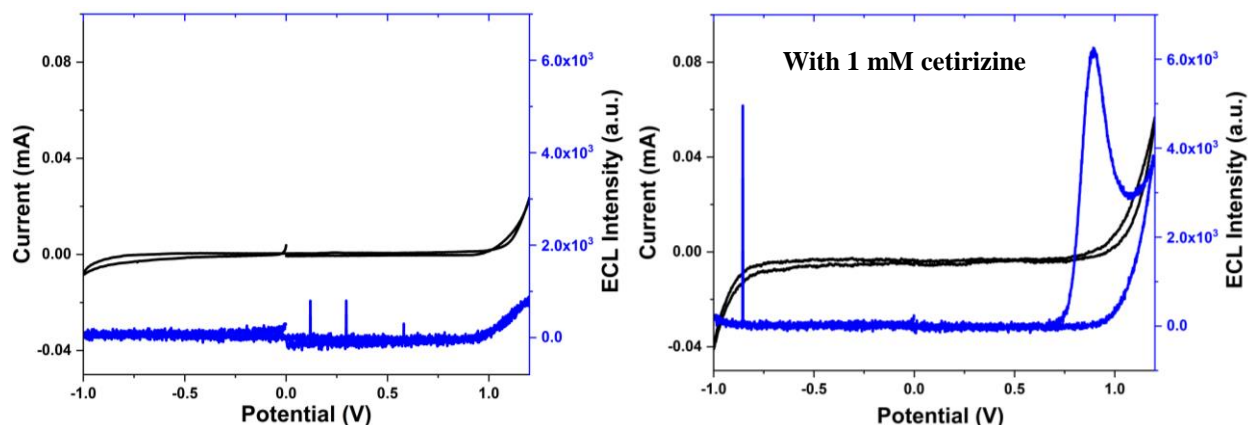


Figure 3.7 The CV-ECL curves of AgAu NCs deposited on ITO working electrode tested without (left) and with (right) 1 mM cetirizine in PBS buffer pH 7.4 . Cyclic voltammogram current in black on left axis, ECL intensity in blue on right axis.

A distinct ECL signal is detected at slightly less than + 1.0 V (updated with the peak potential) with cetirizine added in the measurement solution shown in Figure 3.7. The results clearly demonstrate the signal-on type response to the cetirizine drug and confirm the efficiency of its function as ECL coreactants. Interestingly, the anodic current also increase in the same potential range. A defined current peak could not be resolved limited by possible water/solvent

oxidation that would contribute much higher background current. Therefore, ECL is a more suitable signal for detection of cetirizine over current in the system of Au₁₂Ag₁₃ NCs immobilized on ITO electrodes. The self-annihilation ECL is not observed in CV-ECL, unlike the near IR ECL results in Figure 3.4 generated by potential steps. The difference is explained by the much longer time to sweep the potential within the chosen range of -1 V to 1.2 V in CV, during which the oxidized/reduced intermediate radicals would have undergone various possible side reactions.

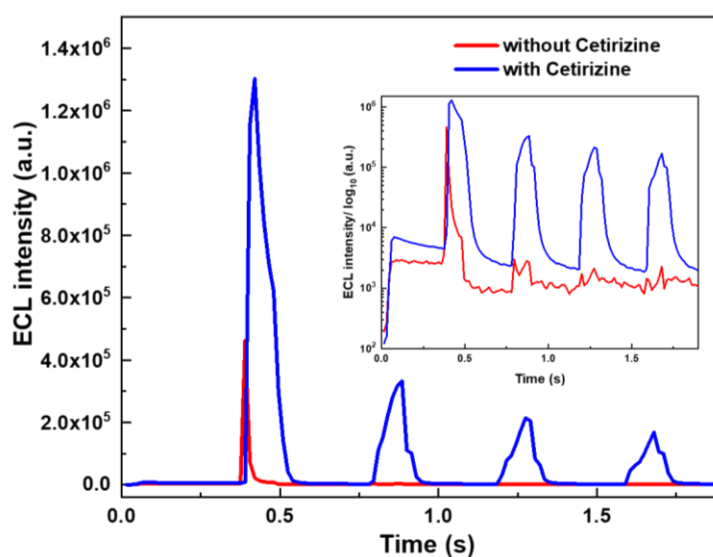


Figure 3.8 Step ECL signals with and without 1 mM Cetirizine in pH 7.4 PBS buffer. The electrode potential was held for 0.3s at -1.0 V (starting from zero second) and then stepped to 1.0 V for 0.1s cyclically. Data with four repeated cycles are plotted. The NCs were deposited by adding 5 μ L drop of stock DCM solution under spin coating speed of 600 RPM ten times.

The impacts of cetirizine on the near IR ECL signal are directly compared under comparable conditions with potential step methods in Figure 3.8. Both peak intensity and duration (peak area, or total ECL intensity) are drastically enhanced by cetirizine. As a reminder, protonation of tertiary amine into quart ammonium ion is known to inhibit the ECL enhancement. At physiological pH 7.4, most nitrogen atoms in cetirizine remain deprotonated

(the pKas of the two amine groups are ca. pKa 2.2 for the one closer to the aromatic rings pKa 8 for the other). The combinations of potential step parameters, -1.0 V for 0.3 s and +1.0 V for 0.1 s, were based on previous surface ECL measurements that remain to be optimized. Generally speaking, applying negative potential first with longer holding time induces higher ECL signal when oxidation potential is applied. A faster potential step/switching is expected to reduce possible side reactions but could also generate less radicals or photons for a given exposure time.

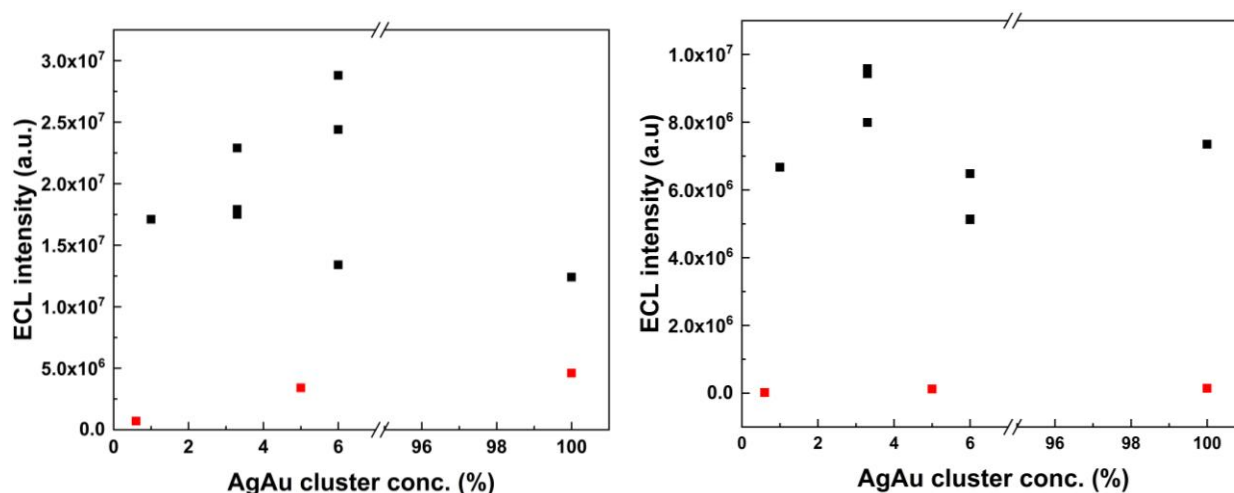


Figure 3.9 Consistency in step ECL signals with respect to the surface deposition: (left) 1st peak and (right) the 3rd peak intensity with cetirizine drug (black) and without (red). The x-axis represents different concentrations of Au₁₂Ag₁₃ NCs used in the spin coating process, with 100% corresponding to the stock solution. Each point represents a separate film/measurement like those in Fig. 3.7 (original data not shown).

Semi-quantitative correlations of the ECL signal with the amount of NCs used in the surface deposition are attempted. Because ECL or electrochemical reaction in general are interfacial processes, it is not necessarily true that higher concentration materials will be better in signal generation. Indeed, decreasing the total amount of NCs deposited did not cause statistically different ECL signals. Better reproducibility is obviously needed to establish a more quantitative trend. Regardless, the ECL signals are distinguishably higher than the signal without

cetirizine in the solution. More consistent surface deposition and optimized measurement parameters are required to establish the calibration profiles for cetirizine or other analytes.

3.4.3 Surface distribution and morphologies of Au₁₂Ag₁₃ NCs on ITO electrodes by spin coating with mixed solvents

The bimetallic Au₁₂Ag₁₃ NCs are less soluble in pure acetonitrile (ACN) compared to other solvent such as DCM. The Au₁₂Ag₁₃ NCs stock solution in DCM (absorbance about 0.6 at 365 nm) was diluted with ACN to 1:1 volume ratio. Besides the slower evaporation rate of the solvent during spin coating, the changes in solvent polarity/affinity will also affect other interactions such as NCs with ITO surface and NCs themselves that affect the surface morphology or assembly pattern, and correspondingly ECL and other properties.

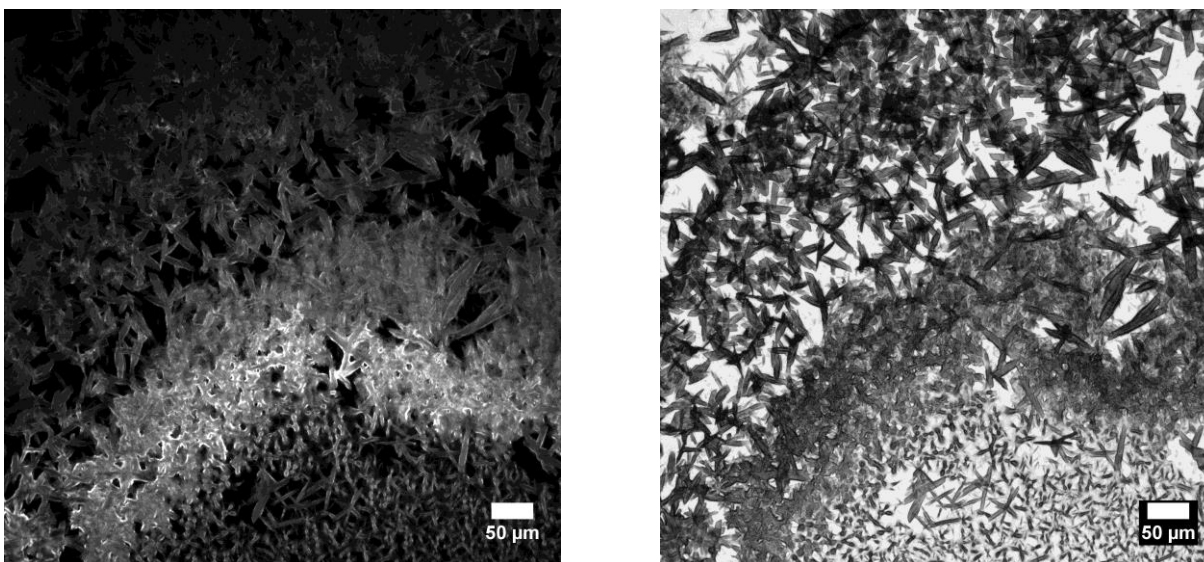


Figure 3.10 Fluorescence (left) and bright field (right) images of surface assembled NCs prepared by spin coating with 1:1 of ACN:DCM as mixed solvent at spin speed 600 RPM. Three drops of 3 μ L solution was used to form the microcrystal assembly.

When spin coated with mixed solvent DCM and ACN, the Au₁₂Ag₁₃ NCs self-assemble into microcrystals on the ITO surface shown in Figure 3.10. It is important to emphasize that neither NCs microcrystals and/or ordered assemblies on surface nor their solid-state

photoluminescence have been previously observed. The results herein open a new paradigm to study these fascinating atomically precise nanoclusters, both from fundamental perspective and for potential applications based on their physiochemical properties. The dimension of individual microcrystals, the distribution and coverage of the microcrystals, as well as their assembly conditions needs to be optimized in future studies. Those will likely depend on parameters such as the solvent ratio, NCs concentration and spin speed and ITO electrode surface preparations etc.

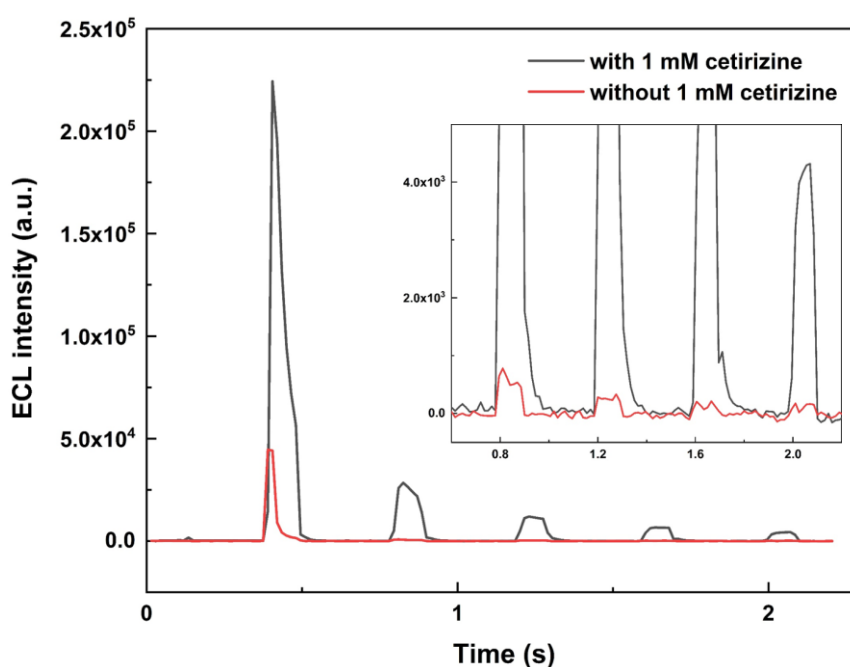


Figure 3.11 ECL profile of the NCs microcrystals (shown in Fig. 3.9) in 1 mM Cetirizine (black) and without cetirizine (red) in pH 7.4 PBS buffer. Insert is zoom-in of later four cycles for better demonstration the ECL signal without cetirizine. The electrode potential was held for 0.3s at -1.0 V and then step to 1.0 V for 0.1s cyclically.

Among many exciting properties to explore on the microcrystals and assemblies, ECL is more relevant to this thesis and tested preliminarily. The self-annihilation ECL is weak but detectable. The enhanced ECL by 1 mM cetirizine is shown in Figure 3.11. Qualitatively, the ECL features are similar to other surface deposited NCs with amorphous structures, displaying a

peak by stepping to positive potentials followed by a gradual decay. More quantitative comparison will require systematic measurements and characterization of the surface concentration or amount of NCs.

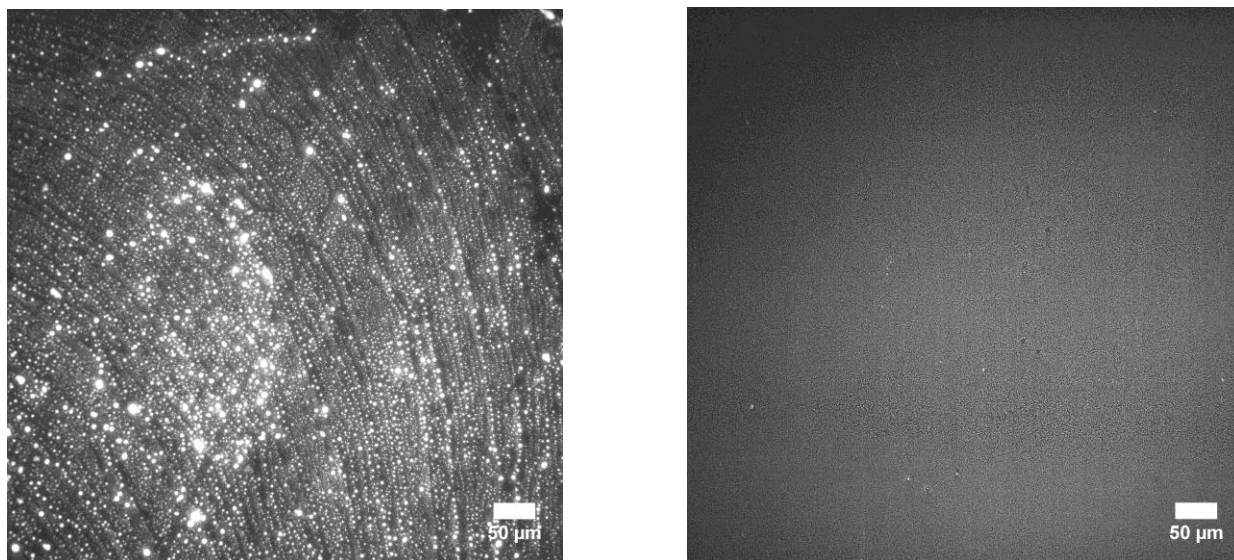


Figure 3.12 , Fluorescence images of surface assembled NCs prepared by spin coating with 1:1 DCM: chloroform as mixed solvent at spin speed 600 RPM (left) and 900 RPM (right).

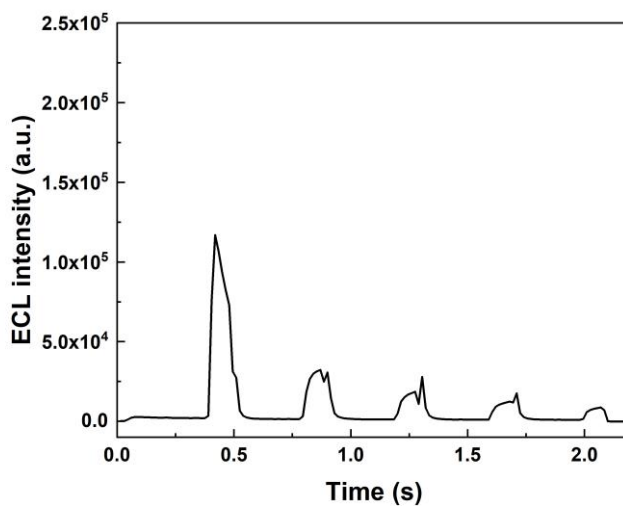


Figure 3.13 ECL profile of the surface assembled NCs prepared by spin coating with 1:1 DCM: chloroform as mixed solvent. Measured in 1 mM Cetirizine in pH 7.4 PBS buffer. The electrode potential was held for 0.3s at -1.0 V and then step to 1.0 V for 0.1s cyclically.

Higher surface coverage and more uniform films are obtained by spin coating with mixed DCM: chloroform at 1:1 volume ratio. The solubility of Au₁₂Ag₁₃ NCs in DCM and chloroform

is similar. Therefore, the changes in solvent affinity/interactions with NCs or ITO surface are expected to be insignificant. From the images in Figure 3.12, no microcrystals could be observed. The slower solvent evaporation rate allows better NCs-ITO interactions which produces better surface distribution and coverage. In the left image, extra sample volume and accumulated dry spots under slow spin speed are clearly visible. By adopting faster spin speed and less drop volume (900 RPM & 3 μ L), highly uniform film across a large coverage area around 0.5 cm² was deposit on the ITO electrode. The right image is representative of the whole ITO in which only few brighter spots are present over a large view area. Note the whole area is emissive and thus no contrast is available within the image; those brighter spots correspond to the few aggregates of the NCs over the highly uniform emissive film (not dark background) that is further explained in the next section.

ECL from this NCs film display similar qualitative features compared to other surface deposited NCs. Cetirizine again is found to enhance the near IR ECL signal shown in Figure 3.13. Quantitative and systematic characterizations will be performed in future studies.

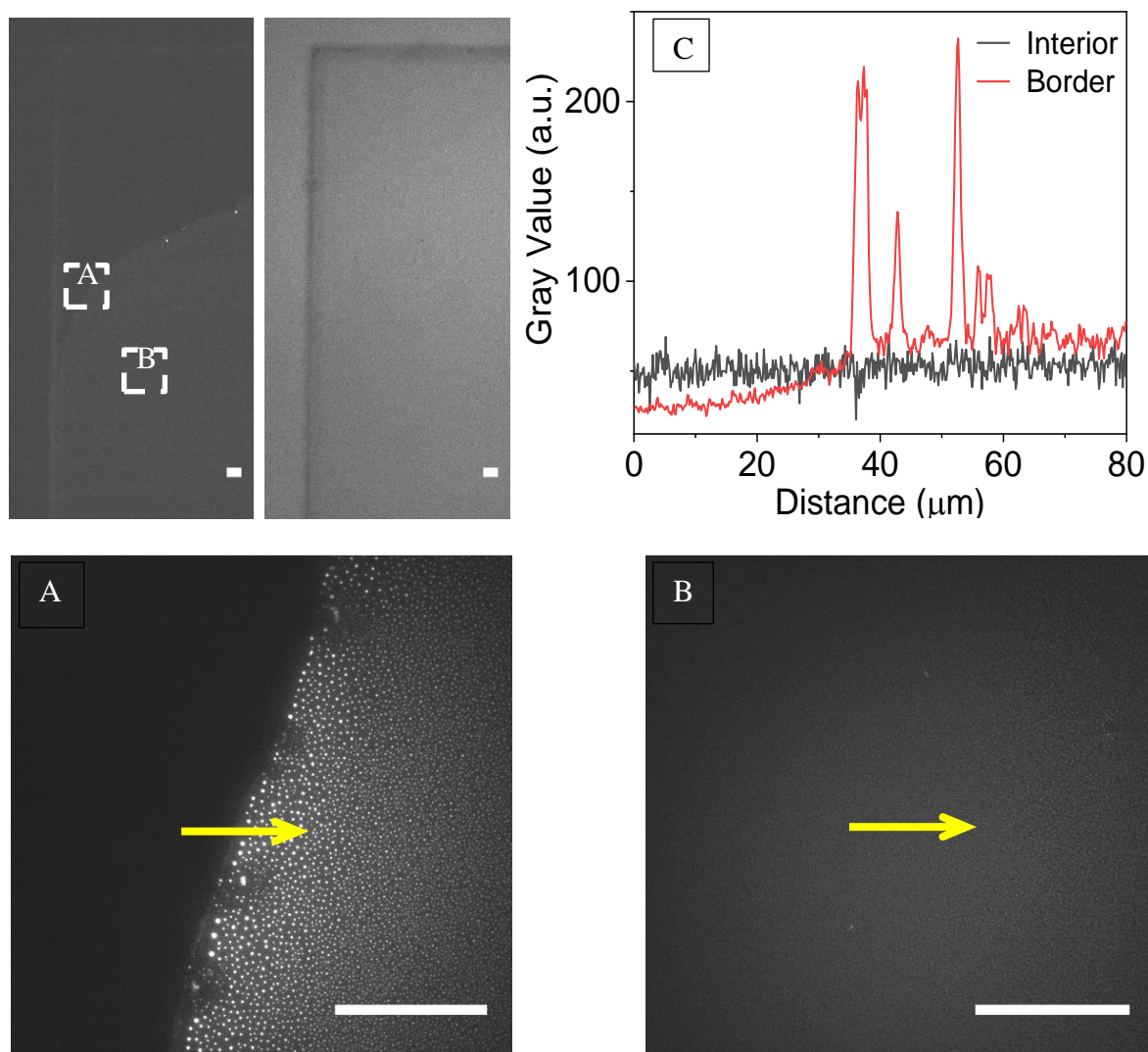


Figure 3.14 The homogeneity analysis of NCs film on ITO. The top left panel provides an overview of ITO slide including the physical edge under fluorescence (left) and bright field (right) mode. The two fluorescence images at the bottom provide zoom-in area of (A) the edge of the NCs film; and (B) the interior of the NCs film. Spin coating speed was 900 RPM. Scale bar size is 100 μm in all images. The two-line profiles in analysis (C) are the emission intensity along the yellow arrows in image A and B respectively. Distance zero is the start of the arrow from the left. NCs film prepared by spin coating a single 3 μL drop NCs solution with 1: 1 DCM: chloroform solvent.

To better illustrate the uniformness of the NCs film prepared with the introduction of chloroform, more quantitative image analysis is summarized in Figure 3.14. The edge of ITO and the edge of the NCs surface film are purposely included as contrast. The red line profile in

panel C at the distance $< 20 \mu\text{m}$ is outside of the NCs film. This low photon counts and less 'noisy' region, statistically significant, serves as the background contrast. The high intensity peaks in the red profile are the bright spots near the edge of the NCs film corresponding to evaporation induce aggregates. The intensity of the interior film, i.e. area B, is highly consistent (at around 50 a.u. herein). The rms 'noise' level is also higher than the blank ITO where no emissive NCs are available. This does not indicate inhomogeneity but results from the optical diffraction limit and the hardware (camera/optics) resolution at hundreds nanometer which are much larger than the NCs (about $< 2 \text{ nm}$ in core size). The analysis here will be adopted in the future to quantitate films prepared under systematically varied conditions and correlate with ECL and other function studies.

3.5 Conclusion

Bimetallic $\text{Au}_{12}\text{Ag}_{13}$ nanoclusters with record high near IR photoluminescence and ECL in solution are deposited on surface. Microcrystals and highly uniform films on ITO electrodes were fabricated by adopting mixed solvents and optimizing spin coating conditions. Solid state photoluminescence is observed from both the amorphous film and the microcrystal assemblies. Optical imaging and analysis were performed to evaluate the surface coverage, morphology and homogeneity. The high-quality surface assembled NCs structures open a new paradigm to explore a wide array of physicochemical properties. Preliminary tests suggest that the near IR ECL is drastically enhanced by tertiary amine drug cetirizine as coreactants.

4 SUMMARY

Surface deposition strategies are developed to assemble aqueous and organic soluble noble-metal nanoclusters onto electrode surfaces for both fundamental research and future catalytic and sensing applications. Optical transparent ITO working electrodes are used for combined electrochemical and optical characterizations. Electrode oxidation and subsequent photoemission are shown as dual signals resulting from the interplay of metal nanoclusters and prototype piperazine compounds. Lipoic acid stabilized Au₂₂ nanoclusters (Au₂₂-LA₁₂) are found to effectively catalyze the oxidation of HEPES on ITO electrode through solution measurements. Oxidized tertiary amines in those piperazine molecular structures in turn enhance the near infrared ECL from the nanoclusters through coreactant reaction pathway. Both the near IR electrochemiluminescence and anodic current signals increase with HEPES concentration indicating signal-on type sensor responses. Deposition on electrode surface by precipitating the aqueous soluble nanoclusters is performed to retain the catalytic effects and to simplify the diffusional collision reaction pathways involved when the nanoclusters are in solution. The stability and uniformity of the surface assembled nanoclusters are investigated through ECL and fluorescence microscopic imaging. Similar to the solution measurements, ECL and current signals are enhanced by HEPES. Quantitative correlations as calibration profiles suggest avenues for further improvements through optimized surface deposition and measurement conditions. Direct deposition of organic soluble nanoclusters make them immediately applicable to aqueous settings. A bimetallic AgAu nanocluster with high near IR photoluminescence and ECL is deposited on ITO. By spin coating in different solvents, microcrystal assemblies and highly uniform amorphous films are created. The two types of high-quality surface assembly structures open the door for various surface analysis and function studies of the growing library of atomic-

precise nanoclusters. Signal-on responses are demonstrated by the enhanced ECL signals through proof of principle tests of piperazine drug cetirizine. The controlled surface assembly and ECL results in this thesis lay the foundation for future basic research in combined optical-electrochemical analysis and for applications toward tertiary amine drug sensing.

REFERENCES

1. Murray, R. W., Nanoelectrochemistry: Metal Nanoparticles, Nanoelectrodes, and Nanopores. *Chemical Reviews* **2008**, *108* (7), 2688-2720.
2. Grieshaber, D.; MacKenzie, R.; Vörös, J.; Reimhult, E., Electrochemical Biosensors - Sensor Principles and Architectures. *Sensors (Basel)* **2008**, *8* (3), 1400-1458.
3. Bakker, E.; Telting-Diaz, M., Electrochemical Sensors. *Analytical Chemistry* **2002**, *74* (12), 2781-2800.
4. Dziąbowska, K.; Czaczyk, E.; Nidzworski, D., Application of Electrochemical Methods in Biosensing Technologies. 2018.
5. Wróblewski, W.; Dybko, A.; Malinowska, E.; Brzózka, Z., Towards advanced chemical microsensors—an overview. *Talanta* **2004**, *63* (1), 33-39.
6. Thévenot, D. R.; Toth, K.; Durst, R. A.; Wilson, G. S., Electrochemical biosensors: recommended definitions and classification | International Union of Pure and Applied Chemistry: Physical Chemistry Division, Commission I.7 (Biophysical Chemistry); Analytical Chemistry Division, Commission V.5 (Electroanalytical Chemistry).1. *Biosensors and Bioelectronics* **2001**, *16* (1), 121-131.
7. Elgrishi, N.; Rountree, K. J.; McCarthy, B. D.; Rountree, E. S.; Eisenhart, T. T.; Dempsey, J. L., A Practical Beginner's Guide to Cyclic Voltammetry. *Journal of Chemical Education* **2018**, *95* (2), 197-206.
8. Yoo, E.-H.; Lee, S.-Y., Glucose biosensors: an overview of use in clinical practice. *Sensors (Basel)* **2010**, *10* (5), 4558-4576.
9. Guilbault, G. G.; Lubrano, G. J., An enzyme electrode for the amperometric determination of glucose. *Analytica Chimica Acta* **1973**, *64* (3), 439-455.
10. Heller, A.; Feldman, B., Electrochemical Glucose Sensors and Their Applications in Diabetes Management. *Chemical Reviews* **2008**, *108* (7), 2482-2505.
11. García-Raya, D.; Madueño, R.; Blázquez, M.; Pineda, T., Electrochemistry of Molecule-like Au₂₅ Nanoclusters Protected by Hexanethiolate. *The Journal of Physical Chemistry C* **2009**, *113* (20), 8756-8761.
12. Negishi, Y.; Nobusada, K.; Tsukuda, T., Glutathione-Protected Gold Clusters Revisited: Bridging the Gap between Gold(I)-Thiolate Complexes and Thiolate-Protected Gold Nanocrystals. *Journal of the American Chemical Society* **2005**, *127* (14), 5261-5270.
13. Jin, R., Quantum sized, thiolate-protected gold nanoclusters. *Nanoscale* **2010**, *2* (3), 343-62.
14. Swain, G. M., 5 - Solid Electrode Materials: Pretreatment and Activation. In *Handbook of Electrochemistry*, Zoski, C. G., Ed. Elsevier: Amsterdam, 2007; pp 111-153.
15. Armstrong, N. R.; Carter, C.; Donley, C.; Simmonds, A.; Lee, P.; Brumbach, M.; Kippelen, B.; Domercq, B.; Yoo, S., Interface modification of ITO thin films: organic photovoltaic cells. *Thin Solid Films* **2003**, *445* (2), 342-352.
16. Zhang, L.; Gong, H., A cheap and non-destructive approach to increase coverage/loading of hydrophilic hydroxide on hydrophobic carbon for lightweight and high-performance supercapacitors. *Scientific Reports* **2015**, *5*, 18108.
17. Ederth, J.; Heszler, P.; Hultåker, A.; Niklasson, G. A.; Granqvist, C. G., Indium tin oxide films made from nanoparticles: models for the optical and electrical properties. *Thin Solid Films* **2003**, *445* (2), 199-206.

18. Choi, M.; Jo, K.; Yang, H., Effect of Different Pretreatments on Indium-Tin Oxide Electrodes. *Bulletin of the Korean Chemical Society* **2013**, *34*, 421-425.
19. Brinker, C. J., Dip Coating. In *Chemical Solution Deposition of Functional Oxide Thin Films*, Schneller, T.; Waser, R.; Kosec, M.; Payne, D., Eds. Springer Vienna: Vienna, 2013; pp 233-261.
20. Birnie, D. P., Spin Coating: Art and Science. In *Chemical Solution Deposition of Functional Oxide Thin Films*, Schneller, T.; Waser, R.; Kosec, M.; Payne, D., Eds. Springer Vienna: Vienna, 2013; pp 263-274.
21. Heller, A., Amperometric biosensors. *Current Opinion in Biotechnology* **1996**, *7* (1), 50-54.
22. Miao, W., Electrogenerated Chemiluminescence and Its Biorelated Applications. *Chemical Reviews* **2008**, *108* (7), 2506-2553.
23. Richter, M. M., Electrochemiluminescence (ECL). *Chemical Reviews* **2004**, *104* (6), 3003-3036.
24. Pastore, P.; Badocco, D.; Zanon, F., Influence of nature, concentration and pH of buffer acid-base system on rate determining step of the electrochemiluminescence of Ru(bpy)₃²⁺ with tertiary aliphatic amines. *Electrochimica Acta* **2006**, *51* (25), 5394-5401.
25. Badocco, D.; Zanon, F.; Pastore, P., Use of Ru(bpy)₃²⁺/tertiary aliphatic amine system fast potential pulses electrochemiluminescence at ultramicroelectrodes coupled to electrochemical data for evaluating E° of amine redox couples. *Electrochimica Acta* **2006**, *51* (28), 6442-6450.
26. Wang, T.; Wang, D.; Padelford, J. W.; Jiang, J.; Wang, G., Near-Infrared Electrogenerated Chemiluminescence from Aqueous Soluble Lipoic Acid Au Nanoclusters. *Journal of the American Chemical Society* **2016**, *138* (20), 6380-6383.
27. Wang, T.; Padelford, J. W.; Ma, H.; Gubitosi-Raspino, M. F.; Wang, G., Near-Infrared Electrochemiluminescence from Au Nanoclusters Enhanced by EDTA and Modulated by Ions. *ChemElectroChem* **2017**, *4* (7), 1697-1701.
28. Wang, T.; Ma, H.; Padelford, J. W.; Lobo, E.; Tran, M. T.; Zhao, F.; Fang, N.; Wang, G., Metal ions-modulated near-infrared electrochemiluminescence from Au nanoclusters enhanced by 4-(2-Hydroxyethyl)-1-piperazineethanesulfonic acid at physiological pH. *Electrochimica Acta* **2018**, *282*, 369-376.
29. Baker, M., Nanotechnology imaging probes: smaller and more stable. *Nat Meth* **2010**, *7* (12), 957-962.
30. Bhattacharyya, D.; Shashank, S.; Satnalika, N.; Ankesh, K.; Seung-Hwan, J., Nanotechnology, Big things from a Tiny World: a Review. *International Journal of u- and e-Service, Science and Technology* **2009**, *2*.
31. Zhang, L.; Wang, E., Metal nanoclusters: New fluorescent probes for sensors and bioimaging. *Nano Today* **2014**, *9* (1), 132-157.
32. Daniel, M.-C.; Astruc, D., Gold Nanoparticles: Assembly, Supramolecular Chemistry, Quantum-Size-Related Properties, and Applications toward Biology, Catalysis, and Nanotechnology. *Chemical Reviews* **2004**, *104* (1), 293-346.
33. Hu, M.; Chen, J.; Li, Z.-Y.; Au, L.; Hartland, G. V.; Li, X.; Marquez, M.; Xia, Y., Gold nanostructures: engineering their plasmonic properties for biomedical applications. *Chemical Society Reviews* **2006**, *35* (11), 1084-1094.

34. Walter, M.; Akola, J.; Lopez-Acevedo, O.; Jadzinsky, P. D.; Calero, G.; Ackerson, C. J.; Whetten, R. L.; Gronbeck, H.; Hakkinen, H., A unified view of ligand-protected gold clusters as superatom complexes. *Proc Natl Acad Sci U S A* **2008**, *105* (27), 9157-62.
35. Toshima, N.; Yonezawa, T., Bimetallic nanoparticles—novel materials for chemical and physical applications. *New Journal of Chemistry* **1998**, *22* (11), 1179-1201.
36. Gilroy, K. D.; Ruditskiy, A.; Peng, H.-C.; Qin, D.; Xia, Y., Bimetallic Nanocrystals: Syntheses, Properties, and Applications. *Chemical Reviews* **2016**, *116* (18), 10414-10472.
37. Jiang, J.; Conroy, C. V.; Kvetny, M. M.; Lake, G. J.; Padelford, J. W.; Ahuja, T.; Wang, G., Oxidation at the Core–Ligand Interface of Au Lipoic Acid Nanoclusters That Enhances the Near-IR Luminescence. *The Journal of Physical Chemistry C* **2014**, *118* (35), 20680-20687.
38. Li, L.; Liu, H.; Shen, Y.; Zhang, J.; Zhu, J.-J., Electrogenerated Chemiluminescence of Au Nanoclusters for the Detection of Dopamine. *Analytical Chemistry* **2011**, *83* (3), 661-665.
39. Shang, L.; Azadfar, N.; Stockmar, F.; Send, W.; Trouillet, V.; Bruns, M.; Gerthsen, D.; Nienhaus, G. U., One-pot synthesis of near-infrared fluorescent gold clusters for cellular fluorescence lifetime imaging. *Small* **2011**, *7* (18), 2614-20.
40. Aldeek, F.; Muhammed, M. A. H.; Palui, G.; Zhan, N.; Mattoussi, H., Growth of Highly Fluorescent Polyethylene Glycol- and Zwitterion-Functionalized Gold Nanoclusters. *ACS Nano* **2013**, *7* (3), 2509-2521.
41. Akola, J.; Walter, M.; Whetten, R. L.; Häkkinen, H.; Grönbeck, H., On the Structure of Thiolate-Protected Au₂₅. *Journal of the American Chemical Society* **2008**, *130* (12), 3756-3757.
42. Zhang, J.; Fu, Y.; Conroy, C. V.; Tang, Z.; Li, G.; Zhao, R. Y.; Wang, G., Fluorescence Intensity and Lifetime Cell Imaging with Luminescent Gold Nanoclusters. *The Journal of Physical Chemistry C* **2012**, *116* (50), 26561-26569.
43. Chen, S.; Ma, H.; Padelford, J. W.; Qinchen, W.; Yu, W.; Wang, S.; Zhu, M.; Wang, G., Near Infrared Electrochemiluminescence of Rod-Shape 25-Atom AuAg Nanoclusters That Is Hundreds-Fold Stronger Than That of Ru(bpy)₃ Standard. *Journal of the American Chemical Society* **2019**, *141* (24), 9603-9609.
44. Wang, S.; Meng, X.; Das, A.; Li, T.; Song, Y.; Cao, T.; Zhu, X.; Zhu, M.; Jin, R., A 200-fold Quantum Yield Boost in the Photoluminescence of Silver-Doped Ag_xAu_{25-x} Nanoclusters: The 13 th Silver Atom Matters. *Angewandte Chemie International Edition* **2014**, *53* (9), 2376-2380.
45. FDA, Clinical pharmacology and biopharmaceutics review of cetirizine Research, C. F. D. E. A., Ed. 2010.
46. Hasan, S.; Al Ali, H.; Al-Qubaisi, M.; Zobir Hussein, M.; Ismail, M.; Zainal, Z.; Nazrul Hakim, M., Controlled-release formulation of antihistamine based on cetirizine zinc-layered hydroxide nanocomposites and its effect on histamine release from basophilic leukemia (RBL-2H3) cells. *Int J Nanomedicine* **2012**, *7*, 3351-3363.
47. Testa, B.; Pagliara, A.; Carrupt, P. A., The molecular behaviour of cetirizine. *Clinical & Experimental Allergy* **1997**, *27* (s2), 13-18.